UCSF
UC San Francisco Electronic Theses and Dissertations

Title
Nanofibrous Scaffold Therapy for Regenerative Medicine

Permalink
https://escholarship.org/uc/item/4ww788zf

Author
Zhu, Yiqian

Publication Date
2010

Peer reviewed|Thesis/dissertation

Nanofibrous Scaffold Therapy for Regenerative Medicine

by

Yiqian Zhu

DISSERTATION

Submitted in partial satisfaction of the requirements for the degree of

DOCTOR OF PHILOSOPHY

In

Bioengineering

in the

GRADUATE DIVISION

of the

UNIVERSITY OF CALIFORNIA, SAN FRANCISCO

AND

UNIVERSITY OF CALIFORNIA, BERKELEY

Acknowledgement

I would like to express my gratitude to numerous people who encouraged and supported me throughout my educational career. First off, this manuscript is dedicated to my loving parents, Shanzhu Zhu and Changgen Wu, without whom none of my accomplishments in science or life would be possible. They taught me the importance and benefit of education and have always stood by my side. I am forever thankful for their sacrifices and hard work that provided me with the opportunities to acquire my achievements.

Next, I would like to thank my graduate advisors and mentors, Dr. William L. Young and Dr. Song Li, from whom I've learned almost everything I know about conducting scientific research. I owe a tremendous portion of my success in graduate school to them. Dr. Young was the first person to expose me to scientific research and imparted to me the practical training to develop my own hypotheses and experimental designs. Dr. Song Li gave me the opportunity to work on research in tissue engineering and material science and instructed me on how to build my future career. Without their guidance and encouragement, I would not have been able to accumulate the research and results that form the basis for this dissertation.

I would like to thank all of my collaborators and co-authors: Guoyuan Yang, Julia Chu, Yongmei Chen, Randall Janairo, Rong Zhang, Hua Su, Shyam Patel, Kyle Kurpinski, Xian Li, Fanxia Shen, Kathryn Miller-Jensen, An-chi Tsou, Jeffery Henry, Timothy L. Downing, Benjamin Lee and Joyce Bao. I am thankful for the diligence and knowledge of Aijun Wang, because without his help, I would not be where I am today. I would also like to thank my three undergraduate students: George Kwong, Yuan Fang Fu and Arezu

Haghighi, for their intelligence and help with my experiments. These three students have shown talent and enthusiasm for research. I am sure that they will undoubtedly be able to have wonderful futures and successful careers as graduate or medical students.

It's been an honor and privilege to work with many of the brightest and most devoted researchers in UCSF and UC Berkeley. My appreciation goes to all the lab members from Center for Cerebrovascular Research, at UCSF and the Cell and Tissue Engineering Lab at UC Berkeley who have influenced and contributed to various parts of my dissertation.

Nanofibrous Scaffold Therapy for Regenerative Medicine

by Yiqian Zhu

Abstract

Nanotechnology innovations create an exciting focus for research in regenerative medicine. Nanomaterials, which form the basis of one of the booming fields of nanotechnology, have tremendous potential for tissue engineering. Many common debilitating and life-threatening diseases arise from the loss or dysfunction of specific tissue types in the body, such as peripheral nerve damages, spinal cord injuries and vascular diseases. To date, peripheral nerve, spinal cord, and vascular regeneration remains a significant challenge in regenerative medicine. The use of electrospinning to generate functional nanofibrous scaffolds for tissue regeneration is particularly exciting, as the structure and morphology of electrospun scaffolds can be manipulated to resemble that of extracellular matrix (ECM), therefore creating a more "familiar" environment for the cells. Synthetic polymer scaffolds composed of either homopolymers or copolymers are biocompatible, have configurable mechanical properties, and can be easily incorporated with bioactive molecules and stem cells to promote nerve, spinal cord, and vascular repair. Aligned nanofibers in the scaffold can enhance regeneration in damaged nerves, accelerate axon growth and angiogenesis in spinal cord injuries, and organize cell alignment and stimulate cell organization in vascular remodeling. *In vivo* studies demonstrate that bi-layer aligned nanofibrous scaffolds have considerable

therapeutic effects for tissue regeneration. In addition, nanofibrous scaffolds offer a valuable platform for drug delivery for spinal cord regeneration. Our studies integrate life science and engineering disciplines to create new generations of prosthetic and medical implants with nanotechnology innovations, intended to benefit patient healthcare in the long run.

TABLE OF CONTENTS

LIST OF FIGURES

LIST OF TABLES

Chapter 1.

Introduction

1.1. Nanomaterials and Medicine

"Nanotechnology has given us the tools…to play with the ultimate toy box of nature-atoms and molecules."

——— Prof. Horst Stormer, Nobel Prize Winner

Nanotechnology is defined as "a branch of technology dealing with the manufacture of objects with dimensions of less than 100 nanometres and the manipulation of individual molecules and atoms" [2]. In the past decade nanotechnology has expanded into many scientific fields. Recent applications of nanotechnology in medicine attract much interest and possess unlimited commercialization prospects. Nanomedicine includes basic particles and materials, molecular devices, bio-robots, artificial tissue and organs and *in vivo* nano-molecular computing (Figure 1.1.).

Nanomaterials, one of the booming fields of nanotechnology, not only encourages scientists to design and construct nano-devices used in clinical diagnosis and monitoring but also promotes potential applications in regenerative medicine [7]. Many applications of nanomaterials to biology and medicine include biosensor detection [8-11], DNA structure probing [12], imaging enhancement [13], drug and gene delivery [14-15] and tissue engineering [16-17]. Employing nanoscale biomaterials in tissue engineering includes modifications of surface topography, delivery and release technique, electromechanical systems and scaffold fabrication. These emerging fields can be applied to medical devices and treatment procedures. Most aspects of daily life could potentially benefit from emerging developments in nanomaterials.

Our studies mainly focus on a new generation of prosthetic and medical implants with nanotechnology innovation, intended to benefit patient healthcare in the long run.

2
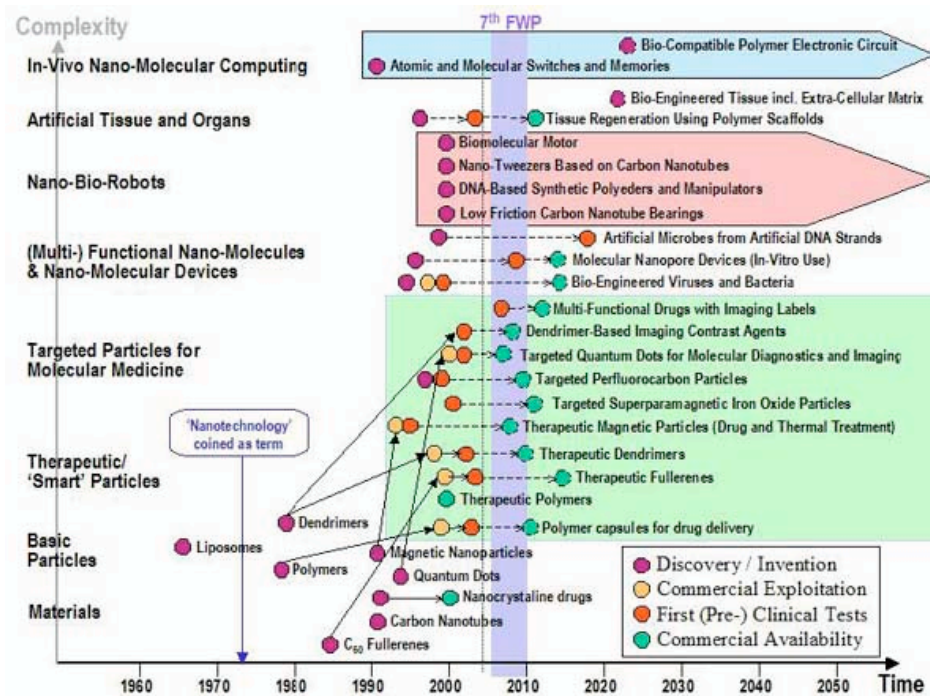
Figure 1.1. Illustration of the achievement and future prospects for nanomedicine. Nanomedicine includes basic particles and materials, molecular devices, bio-robots, artificial tissue and organs and in vivo nano-molecular computing. Image courtesy of Philips Medical Systems.

1.2 Electrospun Nanofibers

Nanotechnology innovations create an exciting focus for research in the tissue-engineering field. Nanomaterials can be used in bio-scaffold construction for providing mechanical support and guidance of cell growth. Recently, the use of the electrospinning technique to generate functional nanofibrous scaffolds for replacing tissues such as nerve, spinal cord or vessels, has been particularly exciting. Biocompatible and biodegradable polymers can be spun into nanofibers in the scaffold to provide

3

mechanical support and guidance of cell growth.

The electrospinning process is outlined as follows: A spinneret is connected to a syringe with a polymer melt solution. A syringe pump controls the flow rate through the spinneret. In general, the polymer solution can be fed at relatively slow rates (less than or equal to 1mL/h). When an external electric field is applied to a charged polymer solution, a suspended conical droplet (Taylor cone) is formed, whereby the surface tension of the droplet is in equilibrium with the force of the electric field. If the electrostatic field overcomes the surface tension of the liquid, a tiny liquid jet is ejected from the surface of the droplet and formed a long and thin thread. As it reaches a grounded mandrel, the jet stream deposits in a grounded collector as fine fibers (Figure
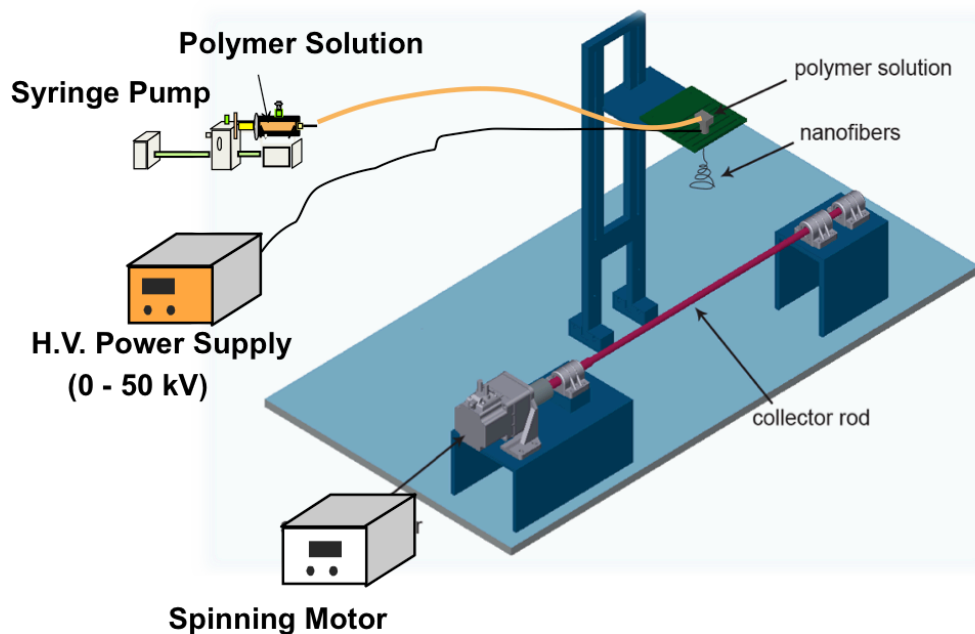
Figure 1.2. Schematic illustration of electrospinning system setup. It is composed of four major components: polymer solution in the syringe pump, a needle spinneret, high-voltage power supply and a grounded collector. Synthetic polymers were used to electrospin nanofibrous scaffolds. Image courtesy of Tsou, D.A. and Li, S. et al., John Wiley & Sons, Inc. 2009 [1].

1.2.). The scaffolds created from these nano-scale fibers (nanofibers) have very large surface area to volume ratios and well-controlled porous structures.

Over the past decade, research has grown to explore the various applications of electro-spun nanofibers. New nano-structured materials have shown significant potential for biomedical applications, including substrates for tissue regeneration and the

Parameter	Effect on fiber morphology
Solution parameter	
Viscosity	Low-bead generation, high-increase in fiber diameter, disappearance of beads.
Polymer concentration	Increase in fiber diameter with increase of concentration.
Molecular weight of polymer	Reduction in the number of beads and droplets with increase of molecular weight.
Conductivity **Surface tension**	Decrease in fiber diameter with increase in conductivity
Processing parameter	
Applied voltage	Decrease in fiber diameter with increase in voltage.
Distance between tip and collector	Generation of beads with too small and too large distance, minimum distance required for uniform fibers.
Feed rate/Flow rate	Decrease in fiber diameter with decrease in flow rate, generation of beads with too high flow rate
Ambient parameters	
Humidity	High humidity results in circular pores on the fibers.
Temperature	Increase in temperature results in decrease in fiber diameter

Table 1.1. The morphology and diameter of electrospun fibers affected by three main factors, namely the solution, processing and ambience. Table courtesy of Bhardwaj, N et al., Biotechnology Advances Jan 2010 [4].

prevention of post-operative induced adhesions [18-22]. The structure and morphology of electrospun nanofibers can be manipulated to resemble that of extracellular matrix (ECM), therefore creating a more "familiar" environment for cells. The use of electrospinning technology allows the creation of 2D and 3D scaffolds with a variety of nanofiber morphologies. Recently we have applied a novel multiple-jet electrospinning process to produce a new type of 3-D nanostructured scaffold for tissue regeneration.

The nanofiber diameter in these scaffolds may range between 50 and 800nm. The morphology and diameter of nanofibers can be controlled by various electrospinning conditions. Three major parameters including solution, processing and ambient parameters can be adjusted in the electrospinning procedure [4]. Solution parameters include viscosity, concentration, molecular weight, conductivity, and surface tension of the polymer [23-24]. Processing parameters include applied voltage, distance between tip and collector and flow rate of polymer solution [21,25]. In addition, ambient parameters consist of humidity and temperature [4]. (Table 1.1.)

1.3. Nanofibrous Material

Electrospinning technology can be used to generate nanofibrous scaffolds made of synthetic polymers as well as native matrix such as collagen and elastin. Synthetic polymer scaffolds such as those composed of lactic or glycolic acids are biocompatible and biodegradable, have configurable mechanical properties and can be easily modified to incorporate proteins and peptides [26-28]. PLA and PGA have been approved by the Food and Drug Administration (FDA) as suture material and use in drug delivery. Recently, copolymer and polymer mixtures have been found to be advantageous over

homopolymers, and can be incorporated to vary the mechanical properties and degradation time of nanofibrous scaffold.

In the past ten years, researchers have shown that electrospun nanofibers of polymers and matrix proteins can support the adhesion and proliferation of endothelial cells (ECs), smooth muscle cells (SMCs) and mesenchymal stem cells (MSCs) [20,29-32]. In addition, nanofibrous scaffolds have large surface area-to-volume ratios, and offer higher capacity for the loading of bioactive molecules to promote tissue regeneration [33]. For example, aligned nanofibers can accelerate axon growth and angiogenesis [16,33-34], and can be used to organize cell alignment and stimulate cell organization in vascular grafts [17]. The natural matrix proteins are not limited by suitable synthetic schemes and have better biocompatibility than synthetic polymers. The ECM protein analogs are comprised of electrospun elastin-like protein reinforced with synthetic collagen to strengthen the mechanical properties in the design of vascular grafts [35].

In Chapters 2 through 4 of our study, we have applied the electrospinning method to design three different nanofibrous scaffolds for peripheral nerve repair, spinal cord regeneration and vascular replacement (Figure 1.3.).

Figure 1.3. Nanofibrous scaffolds for peripheral nerve repair, spinal cord regeneration and vascular replacement. (A) Nerve conduit (B) Spinal cord patch (C) Vascular graft

1.4. Peripheral Nerve Injury and Regeneration

Peripheral nerve injuries are common in both civilian and deployed military personnel populations. They often result from acute trauma and may lead to chronic sensorimotor defects due to the lack of a successful and robust reparative technique. 60 to 70% of all wartime injuries are peripheral nerve injuries [36] and in the civilian population 800,000 peripheral nerve injuries occur annually in the US [37].

The most severe form of injury is a complete nerve transection that results in the loss of sensory and motor functions at the nerve target site. Surgical intervention is necessary to improve the chances of at least the return of partial nerve function. The current gold standard of treatment for a transected nerve with an injury gap is the nerve autograft, a section of nerve harvested from another site in the body [37]. Clinical functional recovery rates typically approach only 80% for nerve injuries treated using autologous nerve grafts. The nerve autograft has the advantages of serving as a physical guide for regenerating nerve fibers [38-39]. Disadvantages of this technique include nerve size mismatches, additional surgery and donor site loss of function and morbidity. Furthermore, in many instances, there is no nerve autograft available.

Several synthetic conduit-shaped nerve guides are currently marketed, but are approved only for short injury gaps (< 3 cm). The designs of these conduits bridging the gap between the severed nerve stumps are similar, but they are composed of either degradable or nondegradable synthetic materials. Nondegradable nerve conduits including silicon and poly (2-hydroxyethyl methacrylate-co-methyl methacrylate) may eventually lead to chronic inflammation, foreign body reactions and tube collapse that induces late nerve compression [40-41]. Biodegradable materials provide an ideal alternative to current clinical nerve injury therapy. Many biodegradable polymers such as

poly (glycolic acid) (PGA) [42-43], poly-caprolactone (PCL) [44] or poly (L-lactic acid) (PLLA) [45], as well as natural biomaterials such as collagen [46], chitosan collagens [47] or keratin [48] have been used as nerve guide materials. These biodegradable and biocompatible conduits could provide a contained semi-permeable environment for nerve fiber growth.

Nerve conduits can accelerate nerve regeneration by directing axonal sprouting from the proximal nerve end [49], preventing scar tissue invasion, and allowing local release of neurotrophic factors to stimulate neural regeneration [37,50]. However, few synthetic products have been shown to outperform the autograft. Advances in nanotechnology and neuroscience provide new opportunities for us to meet this challenge. Electrospinning has been used to fabricate nanofibrous scaffolds from both
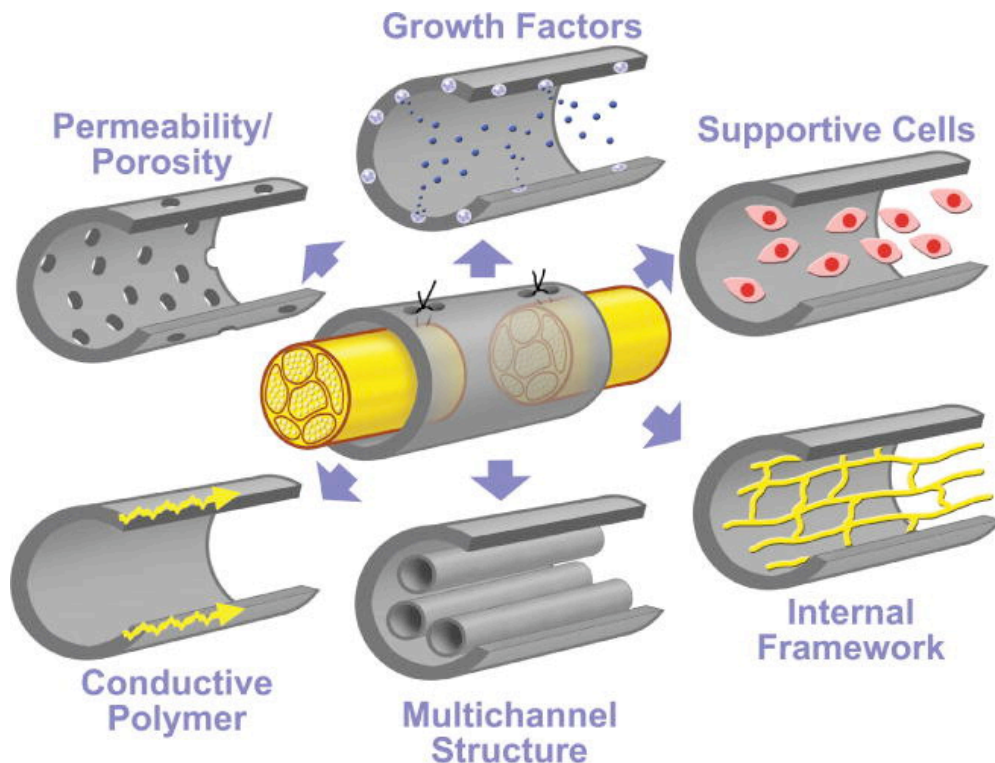
Figure 1.4. Engineering scheme for peripheral nerve regeneration. Image courtesy of de Ruiter, GC et al., Neurosurg Focus Feb 2010 [6].

native matrix and synthetic polymers [25,51-53].

The microenvironment in the nerve conduit plays an important role in peripheral nerve regeneration. Schwann cells migrate from the two nerve ends and eventually form a continuous tissue cable to guides the axons [54]. In addition, schwann cells secrete neurotrophic factors to stimulate axon growth, including nerve growth factor (NGF), brain-derived neurotrophic factor (BDNF), ciliary neurotrophic factor (CNTF) and glial cell line–derived neurotrophic factor (GDNF) [50,55]. Neurotrophic factors such as NGF and BDNF have been shown to provide beneficial effects on the survival of peripheral neuronal cells to promote nerve regeneration [56]. Delivery of neurotrophic factors within nerve grafts has been attempted previously [57-60]. Moreover, neurons could secrete soluble factors to induce the expression of myelin genes in Schwann cells by in vitro co-culture experiments [61].

Generally physical and biochemical guidance cues can enhance nerve growth (Figure 1.4.). Several research publications have studied the use of multichannels and aligned filler materials such as microfilaments, microfibers sutures and magnetically aligned gels to mimic the oriented architecture of the nerve autograft [62-65]. However, the aligned structures in the center of nerve guides have not been shown to enhance functional regeneration in nerve injuries. In contrast, the contact guidance in the lumen wall of the nerve conduit was introduced to enhance nerve regeneration [66].

In Chapter 2, we develop a novel one-step electrospining process that fabricates a seamless bi-layer nanofibrous nerve conduit that is superior to random nanofibrous conduits and has comparable therapeutic effects on autografts for nerve regeneration.

1.5. Spinal Cord Injury and Current Therapy

Spinal cord injury (SCI) and the resulting disability affect more than 200,000 individuals in the United States. To date, spinal cord regeneration remains one of the most challenging problems in regenerative medicine. The difficulty in spinal cord regeneration can be attributed to multiple factors, including the limited regeneration capability of neurons in the central nervous system (CNS), the lack of appropriate axon guidance in the lesion, and inhibitory factors such as myelin breakdown products and chondroitin sulfate proteoglycans (CSPGs) in a glial scar.
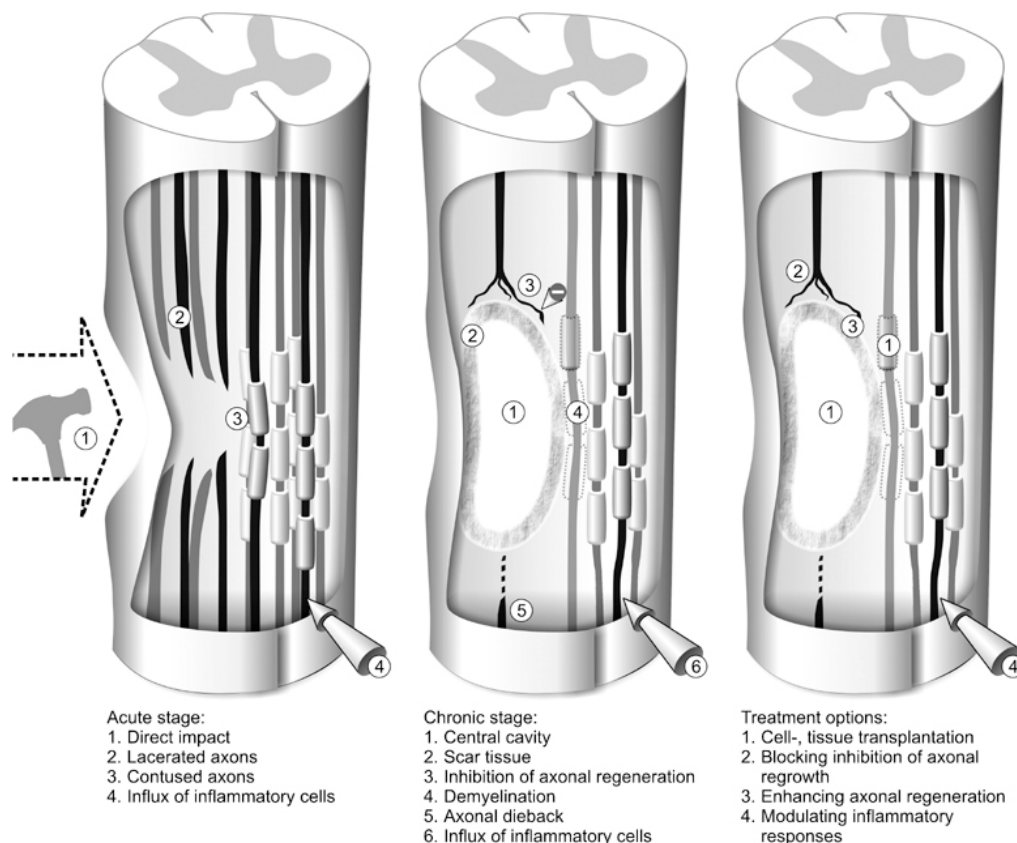
Figure 1.5. **Acute and chronic stages in pathophysiological process of SCI.** Several treatment options are investigated in the current and future study. Image courtesy of Ronsyn, MW et al., Spinal Cord Mar 2008 [3].

Spinal cord injuries not only result in barriers of glial scar and myelin inhibitory molecules, but also cause a physical gap due to the necrosis and apoptosis of cells in the lesion area (Figure 1.5.). Several groups have used scaffolds to bridge the gap in spinal cord lesions [67-70]. However, these scaffolds are either porous scaffolds or hydrogels that do not have nanotopographic guidance cues. Furthermore, drug release has not been incorporated into these scaffolds. Recently, neurotrophic factors such as brain-derived neurotrophic factor (BDNF) and neurotrophin-3 have been released from hydrogels for spinal cord repair [71-72], but strategies to break down the glial scar have not been addressed.

To guide axon growth, we have developed scaffolds with aligned nanofibers (50-800 nm) by using electrospinning technology [16-17,73]. The aligned nanofibrous scaffold not only promotes neuronal guidance, but can also include immobilized bioactive factors. Bioactive factors can be either directly incorporated into nanofibers through co-axial or two-phase electrospinning, or immobilized onto nanofiber surfaces post-electrospinning process [25,53]. Aligned nanofibers immobilized with growth factor can synergistically promote axon growth from dorsal root ganglion (DRG) tissue [16]. The prolonged release of bioactive factors by nanofibrous scaffolds could replace injections or minipump administration of bioactive factors at the lesion site. Rolipram is a selective inhibitor of cyclic AMP phosphodiesterase IV and has antidepressant and anti-inflammatory effects in the central nervous system [74]. Acute rolipram treatment retards the injury-induced increase of IL-1β and TNF-α, which are prominently elevated at the lesion and cause secondary tissue degeneration [75]. Previous investigation has shown increasing cAMP levels in neurons enhance neuronal responsiveness to diffusible growth factor, in order to overcome myelin-associated inhibitory molecules and promote axonal growth and neuritis [76]. In addition, recent evidence suggests rolipram modulates pro-apoptotic caspase 3 activity to provide neuroprotection against several

apoptotic insults [77]. The molecular inhibitors of the injured environment also include chondroitin sulphate proteoglycans (CSPGs) associated with the glial scar, which forms a physical and biochemical barrier to axon growth [78]. Reactive astrocyte-elated astrogliosis contributes to inhibitory extracellular matrix molecules CSPGs expression, which can be reduced with cAMP elevation [79-80]. Rolipram can also prevent hydrolysis of cAMP to induce its accumulation [81].

Recent investigation has reported that axon regrowth is simulated by new blood vessel formation in the damaged tissue after spinal cord injury [82]. Vascular endothelial growth factor (VEGF) induces posttraumatic angiogenesis to improve functional recovery of injured rodents [83]. Targeting microvessel networks may be a valuable therapeutic strategy to optimize treatments for spinal cord injury. The stimulation of prolonged angiogenesis in nanofibrous scaffolds could break new grounds for SCI treatment.

In Chapter 3 of our study, the nanofibrous scaffolds loaded with rolipram are used to bridge the hemisection lesion in order to increase axon growth through the scaffolds and the lesion, as well as promote angiogenesis through the scaffold and decrease the population of astrocytes and CSPGs in the lesion. Our study also demonstrates nanofibrous scaffolds offer a valuable platform for drug delivery for spinal cord regeneration.

1.6. Tissue Engineered Vascular Grafts and Vascular Microenvironment

Cardiovascular diseases is the leading cause of death in the United States. Blood vessel replacement is a common treatment for vascular diseases such as atherosclerosis, restenosis and aneurysm. There are more than 400,000 coronary and 100,000 lower extremity bypass surgeries performed annually. In the past decades, the saphenous vein, which has a 75% 5-year rate, has been the 'gold' standard conduit for

autologous grafting [84]. However, the use of vein grafts is limited by their availability as well as their 15-35% failure rate over ten years. 30% of patients who are in need of bypass surgery do not have a sufficiently suitable saphenous vein due to serious varicose degeneration, previous harvest for bypass surgery, or inadequate diameter or length. In addition, the harvest of a vein graft involves a secondary surgery, additional cost and potential mortality. The development of intimal hyperplasia and accelerated atherosclerosis in vein grafts affected long-term post-operative evaluation [85]. Such medical dilemmas urged many scientists to investigate various biological and synthetic replacements for vein grafts and ameliorate the current shortage situation.

Synthetic vascular grafts are limited to grafts with internal-diameter (ID) larger than 5-mm due to the frequent thrombosis and occlusion in smaller synthetic grafts. Since Weinberg and Bell's landmark report in the vessel model made of Dacron mesh and collagen, there have been various attempts to improve the synthetic vascular grafts, e.g., using poly (ethylene terephthalate), expanded poly (tetrafluoroethylene) and polyurethane [86-87]. To date, no ideal biomaterials are applied in the artificial vascular graft. A previous study has shown a synthetic scaffold composed of poly lactic acid (PLA) has good biocompatibility, biodegradation and mechanical properties [28]. Electrospinning technology can help model synthetic polymer scaffolds that mimic the native matrix. The unique 3-D nanostructured scaffold provides the proper environment for cell growth and tissue generation. The nanofibers, ~500nm in diameter, simulate the structure of native collagen fibrils in the extracellular matrix. In addition, high porosity of the nanofibrous scaffold is ideal for cell infiltration, migration and proliferation. In this study we combined the nanofibrous scaffold and stem cells to fabricate tissue engineered vascular grafts (TEVGs).

In the past decade, TEVGs have had considerable progress with tremendous breakthroughs in cell biology, cell culture and biomaterial improvement. Scientists
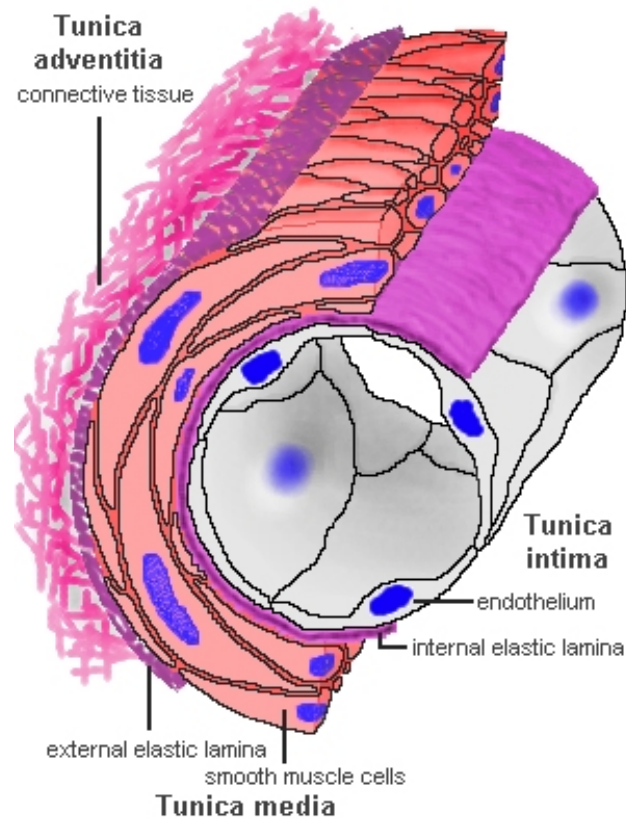
Figure 1.6. Arterial wall depicting three primary layers: intima, media, and adventitia. The major protein components of native artery are collagen and elastin. Image courtesy of Lutz Slomianka's Blue Histology.

continue the pursuit to create a complete TEVG, including three functional layers mimicking that of native blood vessel: the inner endothelial layer, the medial smooth muscle layer and the outer adventitial fibroblast layer (Figure 1.6.). Extracellular matrix components such as collagen, elastin and proteoglycans are the major proteins in the medial and adventitial layers. The three-dimensional (3-D) matrix provides the bulk of the mechanical strength and elastic properties, as well as acts to control vasoactivity. Several groups have established techniques for creating cellular vascular grafts through co-cultures of SMCs and ECs, and successfully produced a completely biological blood

vessel composed of three complete layers, without any exogenous biomaterials [88-89]. Adversely, poor long-term patency in animal experiments is shown in TEVGs without an endothelial cell. An EC monolayer on the inner surface of the vessels prevents platelet adhesion and thrombosis, and regulates SMC contractility. Thus, TEVGs could be a solution to the low patency rate of small-diameter synthetic grafts. In addition to endothelial cells, endothelial progenitor cells (EPCs) exhibit the same characteristics during vascular formation. EPCs could migrate to the regions of the injured endothelial layer and play an important role in vascular wound healing.

The organization of the matrix and cells in TEVGs has not been controlled to stimulate the alignment of SMCs in the circumferential direction of native vessel. Previously we engineered bone marrow derived mesenchymal stem cell (MSCs) on our bioactive and aligned nanofibrous scaffold to investigate structural remodeling and cell organization [17]. However, the cell sources for TEVGs, which need to be non-immunogenic, have not been established. As an alternative to adult stem cells, induced pluripotent stem cells (iPSCs) can potentially provide an unlimited and immune acceptable cell source that may differentiate into vascular cells for the construction of vascular grafts. There is evidence that neural crest stem cells (NCSCs) are a major source of SMCs during vascular development [90-91].

Among biochemical signaling molecules, TGF-β plays a key role in SMC differentiation. TGF-β has been shown to increase SMC marker expression in SMCs [92-94], MSCs [95-96] and adult NCSC lines [97]. However, the effect of TGF-β on iPSC derived NCSCs remains to be determined.

Previously, researchers have produced a tubular tissue structure with the contraction of collagen gel by vascular smooth muscle cells to mimic the media layer in native arteries (Figure 1.7.) [98-100]. In chapter 4, we improve this cellular vascular graft

design and investigate whether the combination of a nanofibrous scaffold, collagen gel and NCSCs enhances the mechanical strength of the graft with TGF-β treatment.
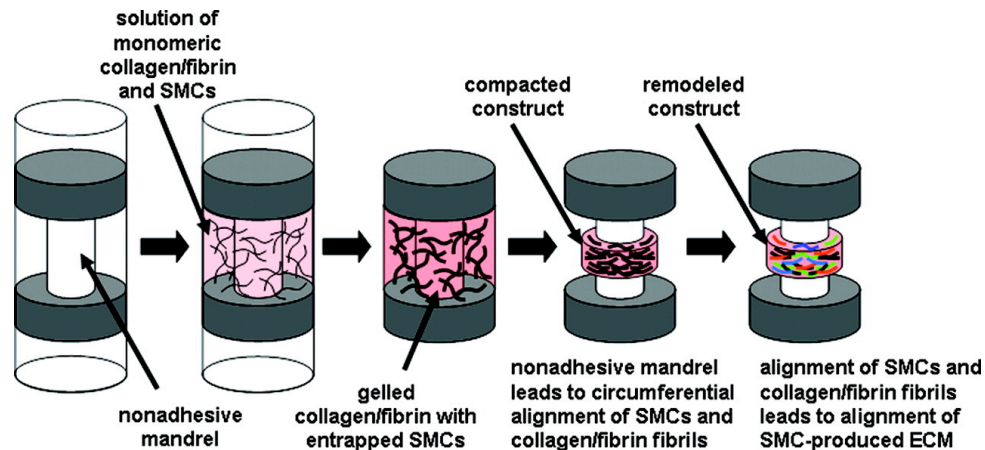
Figure 1.7. Cellular collagen scaffold design. Circumferential alignment attributed to collagen gel and entrapped SMCs contraction. Image courtesy of Isenberg, BC, et al., *Circ Res*. 2006 [5].

1.7. References

[1] Tsou DA, Li S. Engineering microenvironments to control stem cell functions. Emerging Technology Platforms for Stem Cells: John Wiley & Sons, Inc.; 2009. p. 311-26.

[2] The American Heritage dictionary of the English language. 4th ed. Boston: Houghton Mifflin; 2006.

[3] Ronsyn MW, Berneman ZN, Van Tendeloo VF, Jorens PG, Ponsaerts P. Can cell therapy heal a spinal cord injury? Spinal Cord. 2008;46:532-9.

[4] Bhardwaj N, Kundu S. Electrospinning: A fascinating fiber fabrication technique. Biotechnology Advances. 2010;28:22.

[5] Isenberg BC, Williams C, Tranquillo RT. Small-diameter artificial arteries engineered in vitro. Circ Res. 2006;98:25-35.

[6] de Ruiter GC, Malessy MJ, Yaszemski MJ, Windebank AJ, Spinner RJ. Designing ideal conduits for peripheral nerve repair. Neurosurg Focus. 2009;26:E5.

[7] Giersig M, Khomutov GB. Nanomaterials for application in medicine and biology. Dordrecht: Springer; 2008.

[8] Bruchez M, Jr., Moronne M, Gin P, Weiss S, Alivisatos AP. Semiconductor nanocrystals as fluorescent biological labels. Science. 1998;281:2013-6.

[9] Chan WC, Nie S. Quantum dot bioconjugates for ultrasensitive nonisotopic detection. Science. 1998;281:2016-8.

[10] Edelstein RL, Tamanaha CR, Sheehan PE, Miller MM, Baselt DR, Whitman LJ, et al. The BARC biosensor applied to the detection of biological warfare agents. Biosens Bioelectron. 2000;14:805-13.

[11] Nam JM, Thaxton CS, Mirkin CA. Nanoparticle-based bio-bar codes for the ultrasensitive detection of proteins. Science. 2003;301:1884-6.

[12] Seferos DS, Giljohann DA, Hill HD, Prigodich AE, Mirkin CA. Nano-flares: probes for transfection and mRNA detection in living cells. J Am Chem Soc. 2007;129:15477-9.

[13] Weissleder R, Elizondo G, Wittenberg J, Rabito CA, Bengele HH, Josephson L. Ultrasmall superparamagnetic iron oxide: characterization of a new class of contrast agents for MR imaging. Radiology. 1990;175:489-93.

[14] Hansen J, Qing K, Kwon HJ, Mah C, Srivastava A. Impaired intracellular trafficking of adeno-associated virus type 2 vectors limits efficient transduction of murine fibroblasts. J Virol. 2000;74:992-6.

[15] Zhong L, Li B, Jayandharan G, Mah CS, Govindasamy L, Agbandje-McKenna M, et al. Tyrosine-phosphorylation of AAV2 vectors and its consequences on viral intracellular trafficking and transgene expression. Virology. 2008;381:194-202.

[16] Patel S, Kurpinski K, Quigley R, Gao H, Hsiao BS, Poo MM, et al. Bioactive nanofibers: synergistic effects of nanotopography and chemical signaling on cell guidance. Nano Lett. 2007;7:2122-8.

[17] Hashi CK, Zhu Y, Yang GY, Young WL, Hsiao BS, Wang K, et al. Antithrombogenic property of bone marrow mesenchymal stem cells in nanofibrous vascular grafts. Proc Natl Acad Sci U S A. 2007;104:11915-20.

[18] Doshi J, Reneker DH. Electrospinning progress and applications of electrospun fibers. Journal of Electrostatics. 1995;35:151-60.

[19] Boland ED, Wnek GE, Simpson DG, Pawlowski KJ, Bowlin GL. Tailoring tissue engineering scaffolds using electrostatic processing techniques: A study of poly(glycolic acid) electrospinning. Journal of Macromolecular Science-Pure and Applied Chemistry. 2001;38:1231-43.

[20] Huang L, Nagapudi K, Apkarian RP, Chaikof EL. Engineered collagen-PEO nanofibers and fabrics. J Biomater Sci Polym Ed. 2001;12:979-93.

[21] Demir MM, Yilgor I, Yilgo E, Erman B. Electrospinning of polyurethane fibers. Polymer. 2002;43:3303-9.

[22] Zong XH, Ran SF, Fang DF, Hsiao BS, Chu B. Control of structure, morphology and property in electrospun poly (glycolide-co-lactide) non-woven membranes via post-draw treatments. Polymer. 2003;44:4959-67.

[23] Jiang H, Fang D, Hsiao BS, Chu B, Chen W. Optimization and characterization of dextran membranes prepared by electrospinning. Biomacromolecules. 2004;5:326-33.

[24] Chen VJ, Ma PX. Nano-fibrous poly(L-lactic acid) scaffolds with interconnected spherical macropores. Biomaterials. 2004;25:2065-73.

[25] Sill TJ, von Recum HA. Electrospinning: applications in drug delivery and tissue engineering. Biomaterials. 2008;29:1989-2006.

[26] Holder WD, Jr., Gruber HE, Moore AL, Culberson CR, Anderson W, Burg KJ, et al.

Cellular ingrowth and thickness changes in poly-L-lactide and polyglycolide matrices implanted subcutaneously in the rat. J Biomed Mater Res. 1998;41:412-21.

[27] Jain RA. The manufacturing techniques of various drug loaded biodegradable poly(lactide-co-glycolide) (PLGA) devices. Biomaterials. 2000;21:2475-90.

[28] Lu L, Peter SJ, Lyman MD, Lai HL, Leite SM, Tamada JA, et al. In vitro and in vivo degradation of porous poly(DL-lactic-co-glycolic acid) foams. Biomaterials. 2000;21:1837-45.

[29] Matthews JA, Wnek GE, Simpson DG, Bowlin GL. Electrospinning of collagen nanofibers. Biomacromolecules. 2002;3:232-8.

[30] Yoshimoto H, Shin YM, Terai H, Vacanti JP. A biodegradable nanofiber scaffold by electrospinning and its potential for bone tissue engineering. Biomaterials. 2003;24:2077-82.

[31] Kenawy el R, Layman JM, Watkins JR, Bowlin GL, Matthews JA, Simpson DG, et al. Electrospinning of poly(ethylene-co-vinyl alcohol) fibers. Biomaterials. 2003;24:907-13.

[32] Xu C, Inai R, Kotaki M, Ramakrishna S. Electrospun nanofiber fabrication as synthetic extracellular matrix and its potential for vascular tissue engineering. Tissue Eng. 2004;10:1160-8.

[33] Zhu Y, Wang A, Shen W, Patel S, Zhang R, Young WL, et al. Nanofibrous Patches for Spinal Cord Regeneration. Adv Funct Mater. 2010;20

:7.

[34] Kim YT, Haftel VK, Kumar S, Bellamkonda RV. The role of aligned polymer fiber-based constructs in the bridging of long peripheral nerve gaps. Biomaterials. 2008;29:3117-27.

[35] Caves JM, Kumar VA, Martinez AW, Kim J, Ripberger CM, Haller CA, et al. The use of microfiber composites of elastin-like protein matrix reinforced with synthetic collagen in the design of vascular grafts. Biomaterials. 2010;31:7175-82.

[36] Palleschi A. Nerve reconstruction surgeon aims to help more veterans injured in combat 2008.

[37] Belkas JS, Shoichet MS, Midha R. Peripheral nerve regeneration through guidance tubes. Neurol Res. 2004;26:151-60.

[38] Hudson AR, Morris J, Weddell G, Drury A. Peripheral nerve autografts. J Surg Res. 1972;12:267-74.

[39] Martini R. Expression and functional roles of neural cell surface molecules and extracellular matrix components during development and regeneration of peripheral nerves. J Neurocytol. 1994;23:1-28.

[40] Merle M, Dellon AL, Campbell JN, Chang PS. Complications from silicon-polymer intubulation of nerves. Microsurgery. 1989;10:130-3.

[41] Belkas JS, Munro CA, Shoichet MS, Johnston M, Midha R. Long-term in vivo biomechanical properties and biocompatibility of poly(2-hydroxyethyl methacrylate-co-methyl methacrylate) nerve conduits. Biomaterials. 2005;26:1741-9.

[42] Mackinnon SE, Dellon AL. Clinical nerve reconstruction with a bioabsorbable polyglycolic acid tube. Plast Reconstr Surg. 1990;85:419-24.

[43] Kiyotani T, Teramachi M, Takimoto Y, Nakamura T, Shimizu Y, Endo K. Nerve regeneration across a 25-mm gap bridged by a polyglycolic acid-collagen tube: a histological and electrophysiological evaluation of regenerated nerves. Brain Res. 1996;740:66-74.

[44] Bender MD, Bennett JM, Waddell RL, Doctor JS, Marra KG. Multi-channeled biodegradable polymer/CultiSpher composite nerve guides. Biomaterials. 2004;25:1269-78.

[45] Evans GR, Brandt K, Katz S, Chauvin P, Otto L, Bogle M, et al. Bioactive poly(L-lactic acid) conduits seeded with Schwann cells for peripheral nerve regeneration. Biomaterials. 2002;23:841-8.

[46] Archibald SJ, Shefner J, Krarup C, Madison RD. Monkey median nerve repaired by nerve graft or collagen nerve guide tube. J Neurosci. 1995;15:4109-23.

[47] Wang X, Hu W, Cao Y, Yao J, Wu J, Gu X. Dog sciatic nerve regeneration across a 30-mm defect bridged by a chitosan/PGA artificial nerve graft. Brain. 2005;128:1897-910.

[48] Sierpinski P, Garrett J, Ma J, Apel P, Klorig D, Smith T, et al. The use of keratin biomaterials derived from human hair for the promotion of rapid regeneration of peripheral nerves. Biomaterials. 2008;29:118-28.

[49] Miller C, Jeftinija S, Mallapragada S. Micropatterned Schwann cell-seeded biodegradable polymer substrates significantly enhance neurite alignment and outgrowth. Tissue Eng. 2001;7:705-15.

[50] Schmidt CE, Leach JB. Neural tissue engineering: strategies for repair and regeneration. Annu Rev Biomed Eng. 2003;5:293-347.

[51] Li D, Xia Y. Welding and patterning in a flash. Nat Mater. 2004;3:753-4.

[52] Boland ED, Matthews JA, Pawlowski KJ, Simpson DG, Wnek GE, Bowlin GL. Electrospinning collagen and elastin: preliminary vascular tissue engineering. Front Biosci. 2004;9:1422-32.

[53] Liang D, Hsiao BS, Chu B. Functional electrospun nanofibrous scaffolds for biomedical applications. Adv Drug Deliv Rev. 2007;59:1392-412.

[54] Torigoe K, Tanaka HF, Takahashi A, Awaya A, Hashimoto K. Basic behavior of migratory Schwann cells in peripheral nerve regeneration. Exp Neurol. 1996;137:301-8.

[55] Frostick SP, Yin Q, Kemp GJ. Schwann cells, neurotrophic factors, and peripheral nerve regeneration. Microsurgery. 1998;18:397-405.

[56] Terenghi G. Peripheral nerve regeneration and neurotrophic factors. J Anat. 1999;194 (Pt 1):1-14.

[57] Rich KM, Alexander TD, Pryor JC, Hollowell JP. Nerve growth factor enhances

regeneration through silicone chambers. Exp Neurol. 1989;105:162-70.

[58] Hollowell JP, Villadiego A, Rich KM. Sciatic nerve regeneration across gaps within silicone chambers: long-term effects of NGF and consideration of axonal branching. Exp Neurol. 1990;110:45-51.

[59] Utley DS, Lewin SL, Cheng ET, Verity AN, Sierra D, Terris DJ. Brain-derived neurotrophic factor and collagen tubulization enhance functional recovery after peripheral nerve transection and repair. Arch Otolaryngol Head Neck Surg. 1996;122:407-13.

[60] Shirley DM, Williams SA, Santos PM. Brain-derived neurotrophic factor and peripheral nerve regeneration: a functional evaluation. Laryngoscope. 1996;106:629-32.

[61] Bolin LM, Shooter EM. Neurons regulate Schwann cell genes by diffusible molecules. J Cell Biol. 1993;123:237-43.

[62] Hadlock T, Elisseeff J, Langer R, Vacanti J, Cheney M. A tissue-engineered conduit for peripheral nerve repair. Arch Otolaryngol Head Neck Surg. 1998;124:1081-6.

[63] Sundback C, Hadlock T, Cheney M, Vacanti J. Manufacture of porous polymer nerve conduits by a novel low-pressure injection molding process. Biomaterials. 2003;24:819-30.

[64] Ngo TT, Waggoner PJ, Romero AA, Nelson KD, Eberhart RC, Smith GM. Poly(L-Lactide) microfilaments enhance peripheral nerve regeneration across extended nerve lesions. J Neurosci Res. 2003;72:227-38.

[65] Ceballos D, Navarro X, Dubey N, Wendelschafer-Crabb G, Kennedy WR, Tranquillo RT. Magnetically aligned collagen gel filling a collagen nerve guide improves peripheral nerve regeneration. Exp Neurol. 1999;158:290-300.

[66] Chew SY, Mi R, Hoke A, Leong KW. Aligned Protein-Polymer Composite Fibers Enhance Nerve Regeneration: A Potential Tissue-Engineering Platform. Adv Funct Mater. 2007;17:1288-96.

23

[67] Teng YD, Lavik EB, Qu X, Park KI, Ourednik J, Zurakowski D, et al. Functional recovery following traumatic spinal cord injury mediated by a unique polymer scaffold seeded with neural stem cells. Proc Natl Acad Sci U S A. 2002;99:3024-9.

[68] Tysseling-Mattiace VM, Sahni V, Niece KL, Birch D, Czeisler C, Fehlings MG, et al. Self-assembling nanofibers inhibit glial scar formation and promote axon elongation after spinal cord injury. J Neurosci. 2008;28:3814-23.

[69] Oudega M, Gautier SE, Chapon P, Fragoso M, Bates ML, Parel JM, et al. Axonal regeneration into Schwann cell grafts within resorbable poly(alpha-hydroxyacid) guidance channels in the adult rat spinal cord. Biomaterials. 2001;22:1125-36.

[70] Friedman JA, Windebank AJ, Moore MJ, Spinner RJ, Currier BL, Yaszemski MJ. Biodegradable polymer grafts for surgical repair of the injured spinal cord. Neurosurgery. 2002;51:742-51; discussion 51-2.

[71] Jain A, Kim YT, McKeon RJ, Bellamkonda RV. In situ gelling hydrogels for conformal repair of spinal cord defects, and local delivery of BDNF after spinal cord injury. Biomaterials. 2006;27:497-504.

[72] Taylor SJ, Rosenzweig ES, McDonald JW, 3rd, Sakiyama-Elbert SE. Delivery of neurotrophin-3 from fibrin enhances neuronal fiber sprouting after spinal cord injury. J Control Release. 2006;113:226-35.

[73] Huang NF, Patel S, Thakar RG, Wu J, Hsiao BS, Chu B, et al. Myotube assembly on nanofibrous and micropatterned polymers. Nano Lett. 2006;6:537-42.

[74] Griswold DE, Webb EF, Breton J, White JR, Marshall PJ, Torphy TJ. Effect of selective phosphodiesterase type IV inhibitor, rolipram, on fluid and cellular phases of inflammatory response. Inflammation. 1993;17:333-44.

[75] Koopmans GC, Deumens R, Buss A, Geoghegan L, Myint AM, Honig WH, et al. Acute rolipram/thalidomide treatment improves tissue sparing and locomotion after experimental spinal cord injury. Exp Neurol. 2009.

[76] Domeniconi M, Filbin MT. Overcoming inhibitors in myelin to promote axonal regeneration. J Neurol Sci. 2005;233:43-7.

[77] Chen RW, Williams AJ, Liao Z, Yao C, Tortella FC, Dave JR. Broad spectrum neuroprotection profile of phosphodiesterase inhibitors as related to modulation of cell-cycle elements and caspase-3 activation. Neurosci Lett. 2007;418:165-9.

[78] Jones LL, Sajed D, Tuszynski MH. Axonal regeneration through regions of chondroitin sulfate proteoglycan deposition after spinal cord injury: a balance of permissiveness and inhibition. J Neurosci. 2003;23:9276-88.

[79] McKeon RJ, Schreiber RC, Rudge JS, Silver J. Reduction of neurite outgrowth in a model of glial scarring following CNS injury is correlated with the expression of inhibitory molecules on reactive astrocytes. J Neurosci. 1991;11:3398-411.

[80] Chaudhry N, Filbin MT. Myelin-associated inhibitory signaling and strategies to overcome inhibition. J Cereb Blood Flow Metab. 2007;27:1096-107.

[81] Pearse DD, Pereira FC, Marcillo AE, Bates ML, Berrocal YA, Filbin MT, et al. cAMP and Schwann cells promote axonal growth and functional recovery after spinal cord injury. Nat Med. 2004;10:610-6.

[82] Dray C, Rougon G, Debarbieux F. Quantitative analysis by in vivo imaging of the dynamics of vascular and axonal networks in injured mouse spinal cord. Proc Natl Acad Sci U S A. 2009;106:9459-64.

[83] Widenfalk J, Lipson A, Jubran M, Hofstetter C, Ebendal T, Cao Y, et al. Vascular endothelial growth factor improves functional outcome and decreases secondary degeneration in experimental spinal cord contusion injury. Neuroscience. 2003;120:951-60.

[84] Taylor LM, Jr., Edwards JM, Porter JM. Present status of reversed vein bypass grafting: five-year results of a modern series. J Vasc Surg. 1990;11:193-205; discussion -6.

[85] Davies MG, Hagen PO. Pathophysiology of vein graft failure: a review. Eur J Vasc Endovasc Surg. 1995;9:7-18.

[86] Weinberg CB, Bell E. A blood vessel model constructed from collagen and cultured vascular cells. Science. 1986;231:397-400.

[87] Zdrahala RJ. Small caliber vascular grafts. Part II: Polyurethanes revisited. J Biomater Appl. 1996;11:37-61.

[88] L'Heureux N, Paquet S, Labbe R, Germain L, Auger FA. A completely biological tissue-engineered human blood vessel. FASEB J. 1998;12:47-56.

[89] Niklason LE, Gao J, Abbott WM, Hirschi KK, Houser S, Marini R, et al. Functional arteries grown in vitro. Science. 1999;284:489-93.

[90] Hirschi KK, Majesky MW. Smooth muscle stem cells. Anat Rec A Discov Mol Cell Evol Biol. 2004;276:22-33.

[91] Majesky MW. Developmental basis of vascular smooth muscle diversity. Arterioscler Thromb Vasc Biol. 2007;27:1248-58.

[92] Adam PJ, Regan CP, Hautmann MB, Owens GK. Positive- and negative-acting Kruppel-like transcription factors bind a transforming growth factor beta control element required for expression of the smooth muscle cell differentiation marker SM22alpha in vivo. J Biol Chem. 2000;275:37798-806.

[93] Liu Y, Sinha S, Owens G. A transforming growth factor-beta control element required for SM alpha-actin expression in vivo also partially mediates GKLF-dependent transcriptional repression. J Biol Chem. 2003;278:48004-11.

[94] Hirschi KK, Lai L, Belaguli NS, Dean DA, Schwartz RJ, Zimmer WE. Transforming growth factor-beta induction of smooth muscle cell phenotpye requires transcriptional and post-transcriptional control of serum response factor. J Biol Chem. 2002;277:6287-95.

[95] Kinner B, Zaleskas JM, Spector M. Regulation of smooth muscle actin expression

and contraction in adult human mesenchymal stem cells. Exp Cell Res. 2002;278:72-83.

[96] Wang D, Park JS, Chu JS, Krakowski A, Luo K, Chen DJ, et al. Proteomic profiling of bone marrow mesenchymal stem cells upon transforming growth factor beta1 stimulation. J Biol Chem. 2004;279:43725-34.

[97] Chen S, Lechleider RJ. Transforming growth factor-beta-induced differentiation of smooth muscle from a neural crest stem cell line. Circ Res. 2004;94:1195-202.

[98] Barocas VH, Girton TS, Tranquillo RT. Engineered alignment in media equivalents: magnetic prealignment and mandrel compaction. J Biomech Eng. 1998;120:660-6.

[99] L'Heureux N, Germain L, Labbe R, Auger FA. In vitro construction of a human blood vessel from cultured vascular cells: a morphologic study. J Vasc Surg. 1993;17:499-509.

[100] Grassl ED, Oegema TR, Tranquillo RT. A fibrin-based arterial media equivalent. J Biomed Mater Res A. 2003;66:550-61.

Chapter 2.

Engineering Bi-layer Nanofibrous Conduits

for Peripheral Nerve Regeneration

[1]Zhu Y, Wang A, Patel S, Kurpinski K, Diao E, Bao X, Kwong G, Young WL, Li S. "Engineering Bi-layer Nanofibrous Conduits for Peripheral Nerve Regeneration", Biomaterials. 2010. Submitted.

2.1. INTRODUCTION

Peripheral nerve damage is common following traumatic injuries. The most severe form of damage is a complete nerve transection, which results in loss of sensory and motor function at the nerve target site. The current gold standard of treatment for a transected nerve is bridging the injury gap with a nerve autologous graft (autograft) harvested from another site in the body [1]. The nerve autograft has the advantage of serving as a physical guide for regenerating nerve fibers [2-3]. Disadvantages of this technique include nerve size mismatches, additional surgery and the loss of function and morbidity at the donor site. Furthermore, in many instances there is no suitable nerve autograft available, especially for nerve transection with a large gap.

In the past three decades, nerve conduits made of synthetic polymers or native matrices have been developed as alternatives to autografts. For example, silicone [4], biodegradable polymers such as poly (glycolic acid) (PGA) [5-6], poly-caprolactone (PLC) [7] or poly (L-lactic acid) (PLLA) [8], as well as natural biomaterials such as collagen [9], chitosan [10-11] or keratin [12], have been used as nerve conduit materials. However, none of these nerve conduits has achieved therapeutic effects comparable to autografts.

It is generally recognized that cues from physical and biochemical guidance can promote nerve growth [13]. In early studies, micropatterned channels and extracellular matrices were used to guide axon growth in specific directions [14-15]. Recently, we and others have shown that electrospun aligned nanofibers can promote axon growth and Schwann cell maturation *in vitro* [16-18] and enhance nerve regeneration *in vivo* [19-21]. However, the fabrication of seamless nerve conduits (as opposed to a sheet rolled into a cylindrical shape) with highly aligned nanofibers and clinically relevant mechanical properties has not been realized. Furthermore, the *in vivo* effects of aligned nanofibers

29

on nerve regeneration are inconclusive [19], and the long-term (>6 months) effects of aligned nanofibers on nerve regeneration have not been investigated.

In this study, we developed a one-step procedure to fabricate seamless nerve conduits with a bi-layer structure: the luminal surface has longitudinally aligned nanofibers for nerve guidance and the outer layer has randomly oriented nanofibers for structural support. We evaluated clinically relevant mechanical properties of the electrospun nerve conduit. We systematically compared the long-term (up to 12 months) effects of nerve conduits with autografts in a rat sciatic nerve transection model. Histomorphometry and electrophysiology analysis showed that bi-layer aligned nanofibrous nerve conduits had therapeutic efficacy comparable to autografts. In addition, we demonstrated superior nerve regeneration and muscle function recovery with aligned nanofibrous nerve conduits compared to random nanofibrous nerve conduits.

2.2. MATERIALS AND METHODS

2.2.1. Bi-layer Nerve Conduit Fabrication and Characterization

Nonwoven aligned nanofibrous nerve conduits composed of poly(L-lactide-co-caprolactone) (70:30, Purac Biomaterials, Amsterdam, Netherlands), poly(propylene glycol) (Acros Organics, Morris Plains, NJ) and sodium acetate (Sigma, St. Louis, MO) were fabricated using a customized electrospinning process. The aligned nanofibrous nerve conduits comprised a luminal region of longitudinally aligned nanofibers and an outer region of randomly oriented nanofibers. PLCL, PPG and sodium acetate were dissolved in a volatile organic solvent, hexafluoroisopropanol (HFIP) (Matrix Scientific, Columbia, SC). The electrospinning apparatus consisted of a syringe pump capable of

30

delivering the polymer solution to the tip of a needle secured onto a mechanized platform suspended over a 1.65-mm outer diameter rotating mandrel collector assembly. The needle platform was charged by a positive-polarity power supply and the mandrel assembly was charged by a negative-polarity power supply. Longitudinal fiber alignment was achieved through the design of the rotating mandrel collector assembly. By interspersing electrically insulating polymer sections between electrically conducting stainless steel sections, the mandrel assembly biased deposition of electrospun fibers with orientation parallel to the long axis of the mandrel. After deposition of longitudinally aligned electrospun fibers, subsequent fiber deposition on the mandrel was essentially randomly oriented. The mandrel assembly was rotated around its long axis and the needle was traversed between the ends of the assembly to ensure even fiber deposition.

Upon completion of electrospinning, the nerve conduits were air dried on the steel mandrel for two nights to remove residual HFIP. The nerve conduits were then rinsed in deionized water and cut to appropriate length. Random nanofibrous nerve conduits were fabricated using the same polymer solution but with a uniform stainless steel mandrel as the collector assembly. All nerve conduits were sterilized with ethylene oxide gas before characterization and *in vivo* implantation studies. High and low magnification microscopic images of the electrospun nanofibrous nerve conduits were captured using a Hitachi TM-1000 scanning electron microscope (SEM) (Hitachi U.S.A., Schaumburg, IL). The alignment of the lumen and outer surfaces in nanofibrous nerve conduits was examined by SEM.

2.2.2. *In vivo* Implantation

All animal study procedures were approved by the Institutional Review Board Service and Institutional Animal Care and Use Committee at the University of California, Berkeley. Adult female Lewis rats (250 ± 30 g) were anesthetized with 1.5% isoflurane in

70% N_2O/30% O_2. Body temperature was maintained at 37.0±0.5°C during surgery. Briefly, the rat was set in the left recumbent position, and right gluteal and posterior thigh incisions were made to expose the right sciatic nerve deep to femoris muscle. Under a surgical microscope, 1 cm of the sciatic nerve was excised to obtain the nerve lesion gap. For nerve conduit groups, both nerve ends were inserted 1 mm into the tube lumen and sutured in place with two 10-0 nylon monofilament sutures. For the autograft group, the nerve defect was sutured with a 10-mm reversed nerve segment instead of the nerve conduit. The overlying muscle layers were approximated with interrupted 4-0 nylon sutures and stainless steel wound clips were used to close the skin wound.

The animals were divided into experimental groups according to the composition of the implanted nerve conduits as follows: random nanofibrous nerve conduits (n=12), aligned nanofibrous nerve conduits (n=12) and autograft (a reversed nerve segment) (n=12). In every group, half of the animals were sacrificed 2 months post-surgery, and the other half were maintained for 12 months post-surgery.

2.2.3. Electrophysiology

Electrophysiology analysis was performed at the 2-month and 12-month post-surgery time points. The animals were put in a lateral position and body temperature was maintained at 37°C on a thermostatic pad. The right sciatic nerve was re-exposed through the thigh muscle incision. Bipolar hooked platinum simulating electrodes were placed under the sciatic nerve 5-mm proximal to the graft suturing point. The stimulating electrodes were connected to a pulse generator (SYS-A310, World Precision Instruments Inc., Sarasota, FL) and delivered electrical signals to the nerve. To record the evoked compound muscle action potential (CMAP) signals, a sharp tungsten needle was inserted percutaneously into the midpoint of the right gastrocnemius muscle. A

second tungsten needle probe was positioned subcutaneously over the gastrocnemius muscle. The opposite pole was also grounded to an Ag/AgCl2 electrode placed in a superficial muscle layer near the skin. Signals generated at the tungsten probe were fed to an AC amplifier (DAM-80, WPI) and amplified 10,000 times. The signals were recorded by 4-Channel Data Acquisition System (Lab-Trax-4, WPI) and displayed on a computer monitor. Nerve simulation was elicited using a stimulus fourfold stronger than the original threshold, below which there was no action potential. The amplitude and latency of the action potential waveform were determined to assess the recovery of injured sciatic nerve. Conduction velocities were calculated from derived latencies and the measured distance between the stimulus and recording probes.

2.2.4. Histological Evaluation

At the end of the electrophysiological tests, the animals were sacrificed and sciatic nerve and graft samples were explanted. The tissue samples were fixed with 2.5% glutaraldehyde, 2% paraformaldehyde in 0.1M Sodium Cacodylate (pH 7.2), and post-fixed with 1% osmium tetroxide (Electron Miscroscopy Sciences (EMS), Hatfield, PA) solution. The fixed samples were trimmed, dehydrated stepwise in increasing concentrations of acetone, and embedded in EMbed 812 resin (EMS). Ultra-thin transverse sections were obtained at two sites of a specimen, the midpoint of the graft (5-7 mm from the proximal end of the graft) and the distal nerve tissue (3 mm distal to the coaptation suture site). The samples were sectioned by using a Leica Ultracut E microtome (Leica Microsystems, Germany) at 800-nm thickness, and stained with 1% toluidine blue.

Digitized images of the stained tissue cross-sections were acquired with a Zeiss Axioscope microscope (Zeiss, Thornwood, NY). The thickness of the capsule layer formed outside of the regenerated nerve tissue in the nanofibrous nerve conduits was

measured and compared between aligned and random nanofibrous nerve conduit groups at different time points. Three to five pictures of high-powered fields (15,244 μm^2, at a magnification of 630x) were randomly taken from each sample and myelinated axons with greater than 1-μm^2 area were selected for analysis. This was done for 2-month (n=6) and 12-month (n=6) samples to evaluate axonal regeneration. ImageJ software was used to measure myelinated axon area and myelin sheath thickness at mid-graft regions.

For axon diameter analysis, all axonal shapes were converted into equivalent circles by adjusting the circularity threshold to 0.35 for Image J quantification. This method allowed the inclusion of distorted axons in irregular shape. Equivalent diameters were calculated to generate an axon diameter frequency distribution graph.

To quantify the thickness of myelin sheath, 600 myelinated axons were selected representatively from each picture with high magnification, and the myelin sheath thickness was measured. The frequency distribution of myelin sheath thickness was then generated for each sample group.

2.2.5. Statistical Analysis

For data requiring comparisons between more than two groups, including electrophysiology and fibrous capsule layer, analysis of variance (Statview 5.0) was first used to compare differences between all groups. Post-hoc testing was performed to analyze the data of the electrophysiology and fibrous tissue layer by using Fisher's protected least significant difference (PLSD). A P-value less than 0.05 was considered statistically significant.

2.3. RESULTS

2.3.1. Characterization of Nanofiber Organization in Nerve Conduits

Electrospun nanofibrous nerve conduits with an inner diameter of 1.6 mm were produced (Figure 2.1.A-B). SEM images of the luminal surfaces showed highly aligned nanofibers for the aligned nanofibrous nerve conduits and wavy, randomly oriented nanofibers for the random nanofibrous nerve conduits (Figure 2.1.C-D).
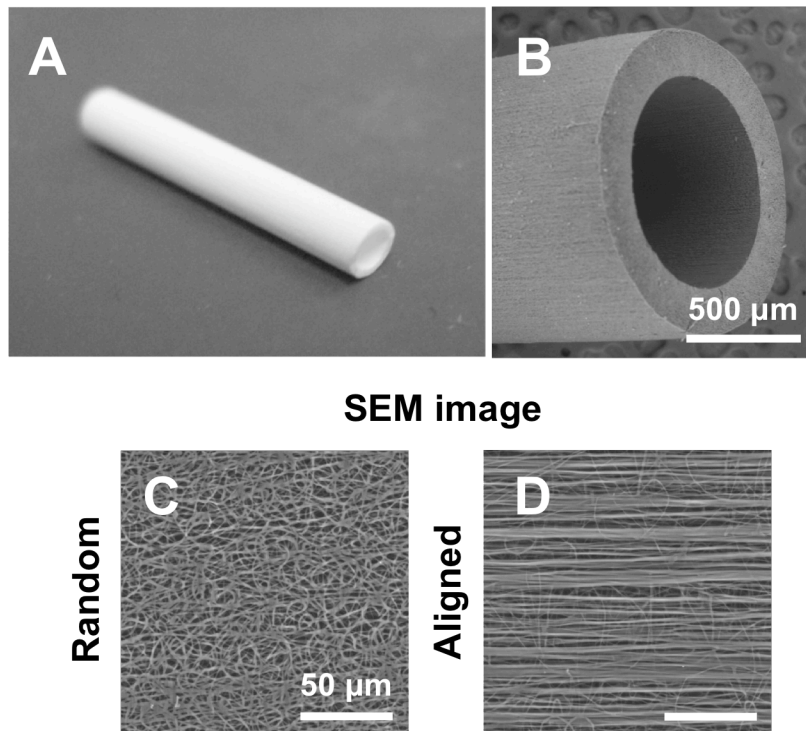
Figure 2.1. Structure of nanofibrous nerve conduit (A) A nanofibrous nerve conduit (1.5cm length, 1.5mm ID). (B) SEM image of a nerve conduit showing aligned fibers in luminal layer and random fibers in outer layer. (C) Alignment analysis of fibers on the luminal surface of nerve conduit (random and aligned).

2.3.2. Electrophysiology Analysis of Nerve Functional Recovery

To quantify the functional recovery of regenerated nerves, electrophysiology analysis was performed at 2-month and 12-month time points to assess the responses of the hindlimb gastrocnemius muscle to electrical stimulation at the proximal end of the grafts. The amplitude and conduction velocity of CMAP were measured and calculated as previously described [10,23]. CMAP amplitude and conduction velocity from the experimental limb were normalized to values from the animal's contralateral control.
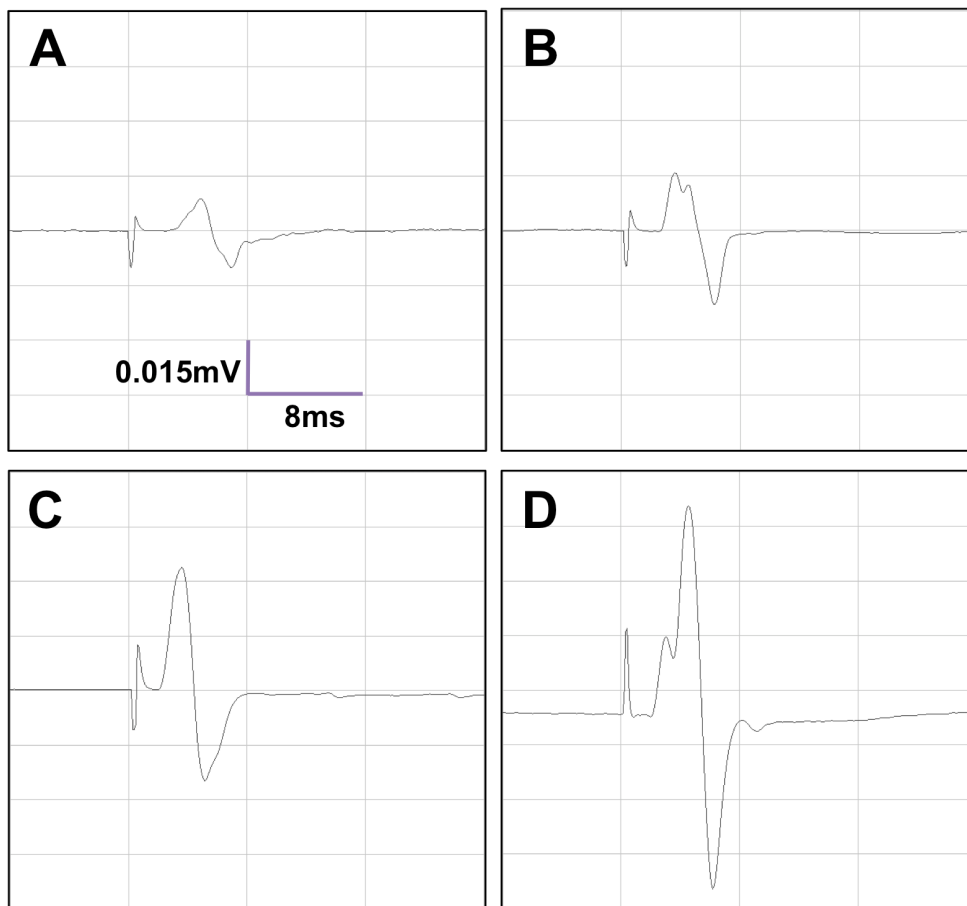
Figure 2.2. Representative electrophysiology data at 12 months. CMAP results recorded at the probe inserted into gastrocnemius muscle of the injury side in the random (A) and aligned (B) nanofibrous nerve conduits, autograft (C) and normal nerve (D) at 12 months.

CMAP amplitude of the aligned nanofibrous conduit group (19.0% ± 5.3%, 45.7% ± 24.9%) showed significantly better functional recovery than the random nanofibrous conduit group (6.5% ± 0.7%, 19.1% ± 8.4%) at 2 and 12 months respectively (P<0.05). CMAP conduction velocity of aligned nanofibrous nerve conduits was also significantly higher than random nanofibrous nerve conduits at 2 and 12 months. There were no statistically significant differences in CMAP amplitude and conduction velocity between the aligned nanofibrous nerve conduit and autograft groups at both the 2-month and 12-month time points (Figure 2.2.). However, at the 2-month time point, autografts did not show a significant improvement in CMAP amplitude and conduction velocity compared to random nanofibrous conduits.
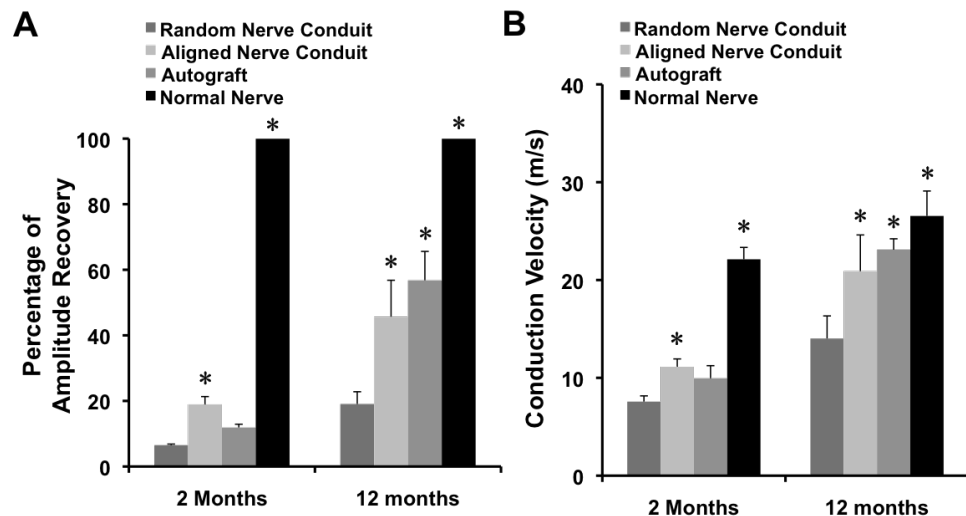
Figure 2.3. Summary of electrophysiology data at 2 and 12 months. (A) Percentage of CMAP amplitude recovery. (B) Comparison of CMAP conduction velocity. * indicates significant difference (P<0.05) compared to the random nanofibrous nerve conduit groups at 2 months and 12 months using Fisher's protected least significant difference (PLSD) (n = 6) and all data was presented as mean ± standard error of the mean (SEM).
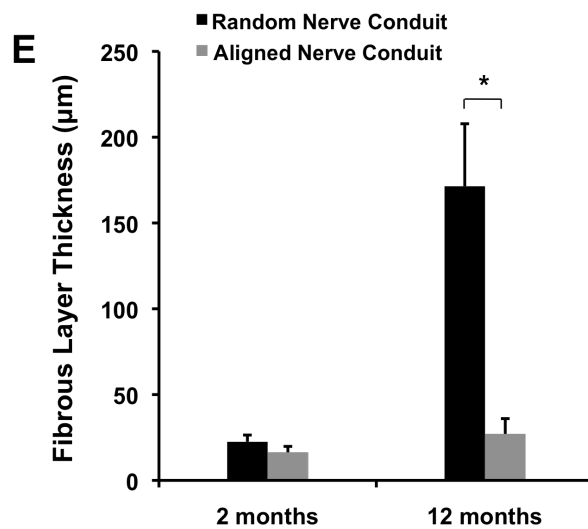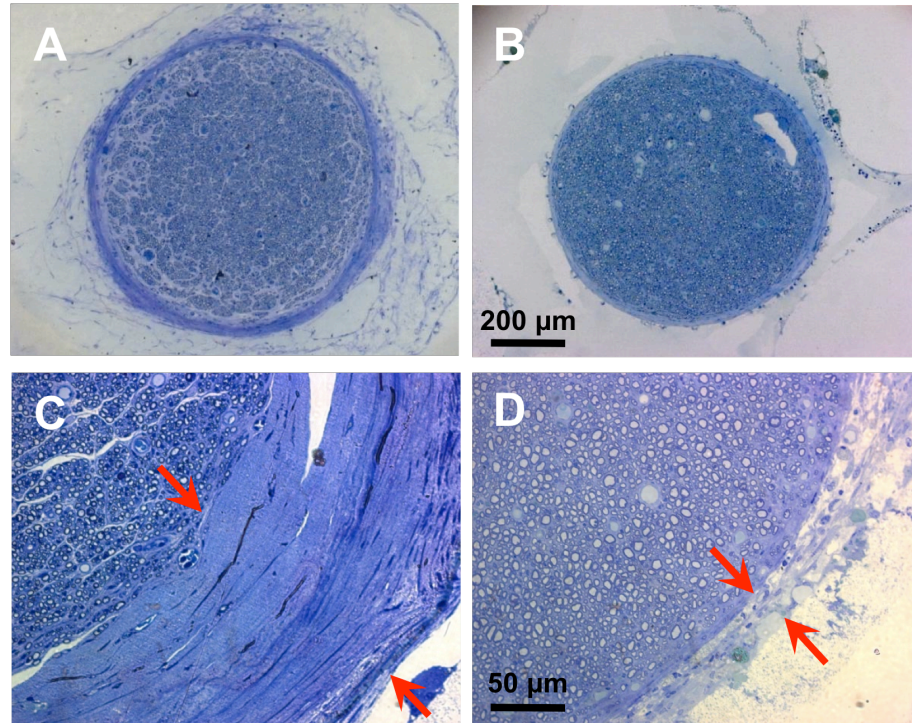
Figure 2.4. Representative micrographs of toluidine-blue staining showing the regenerated nerve and fibrous tissue layer. (A) Random nanofibrous conduit at 2 months. (B) Aligned nanofibrous conduit at 2 months. (C) Random nanofibrous conduit at 12 months. (D) Aligned nanofibrous conduit at 12 months. Arrows indicate the fibrous tissue layer. Scale bar = 50 µm. (E) Quantification of the thickness of the fibrous tissue layer. * indicates significant difference (P<0.05) using two-tailed unpaired t-test and the data was presented as mean ± SD.

Temporally, both CMAP amplitude and conduction velocity in the aligned nanofibrous nerve conduit and autograft groups at 12 months showed significant improvement over the respective 2-month values (Figure 2.3.). For random nanofibrous nerve conduits, conduction velocity, but not CAMP amplitude, at 12 months showed significant improvement over 2-month values.

2.3.3. Effects of Nanofiber Alignment on the Formation of a Fibrous Tissue Layer

After 2 months, electrospun nanofibrous nerve conduits supported axonal regeneration across the 10-mm injury gap. As shown in Figure 2.4, the nerve regenerated in both random (Figure 2.4.A) and aligned (Figure 2.4.B) nanofibrous nerve conduit groups at 2 months post-surgery. Microscopic examination of the luminal surface showed that there was a fibrous tissue sheath at the interface of the nerve and the conduit wall in all nanofibrous conduit samples. In the random nanofibrous nerve conduit group, the fibrous sheath at 12 months was significantly thicker (Figure 2.4.C) than that at 2 months (Figure 2.4.A, E), demonstrating significant growth between 2 and 12-month time points. In contrast, regenerated nerves in the aligned nanofibrous conduit group displayed an epineurial-like fibrous sheath with similar thicknesses at both 2-month and 12-month time points (Figure 2.4.B, D), significantly less than that in random nanofibrous conduits at 12 months.

2.3.4. Histomorphometry of Regenerated Nerves

To quantitatively compare the regenerated nerves, histomorphometric analysis of toluidine blue-stained cross sections was performed on 2-month and 12-month samples. Myelinated axons were observed in cross-sections from the middle portion of grafts

(mid-graft) and distal nerve segments of all samples at the 2-month and 12-month time points: random nanofibrous nerve conduit group (Figure 2.5.A,D), aligned nanofibrous nerve conduit group (Figure 2.5.B,E) and autograft group (Figure 2.5.C,F). Vascularization of the regenerated nerve tissue was also observed and was similar in all samples (data not shown). Quantitative analysis of mid-graft cross-sections was performed to measure regenerated axon diameter and myelin sheath thickness. Axon diameter (Figure 2.7.) and myelin sheath thickness (Figure 2.7.) were plotted as a frequency distribution based on the dimension.
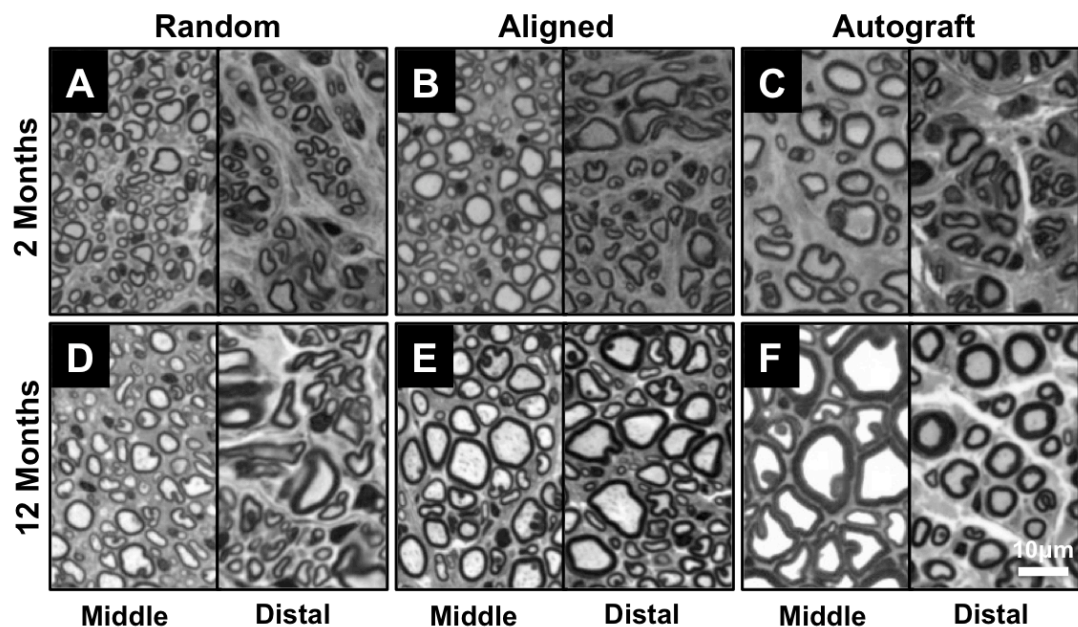
Figure 2.5. Representative micrographs of toluidine-blue stained cross-sections of 2-month (A, B, C) and 12-month (D, E, F) samples. (A, D) Radom nanofibrous nerve conduit group; (B, E) Aligned nanofibrous nerve conduit group; (C, F) Autograft group. The middle (left panel) and distal (right panel) portions of representative grafts are shown. Scale bar = 20 μm.

At 2 months, both the aligned nanofibrous nerve conduit and autograft groups displayed higher frequencies of large axons (3–6 μm in diameter) than the random

nanofibrous nerve conduit group (Figure 2.6.). Aligned nanofibrous nerve conduit and

autograft groups also displayed higher frequencies of thick myelin sheaths (>0.8 μm)

than the random nanofibrous nerve conduit group (Figure 2.7.). The aligned nanofibrous
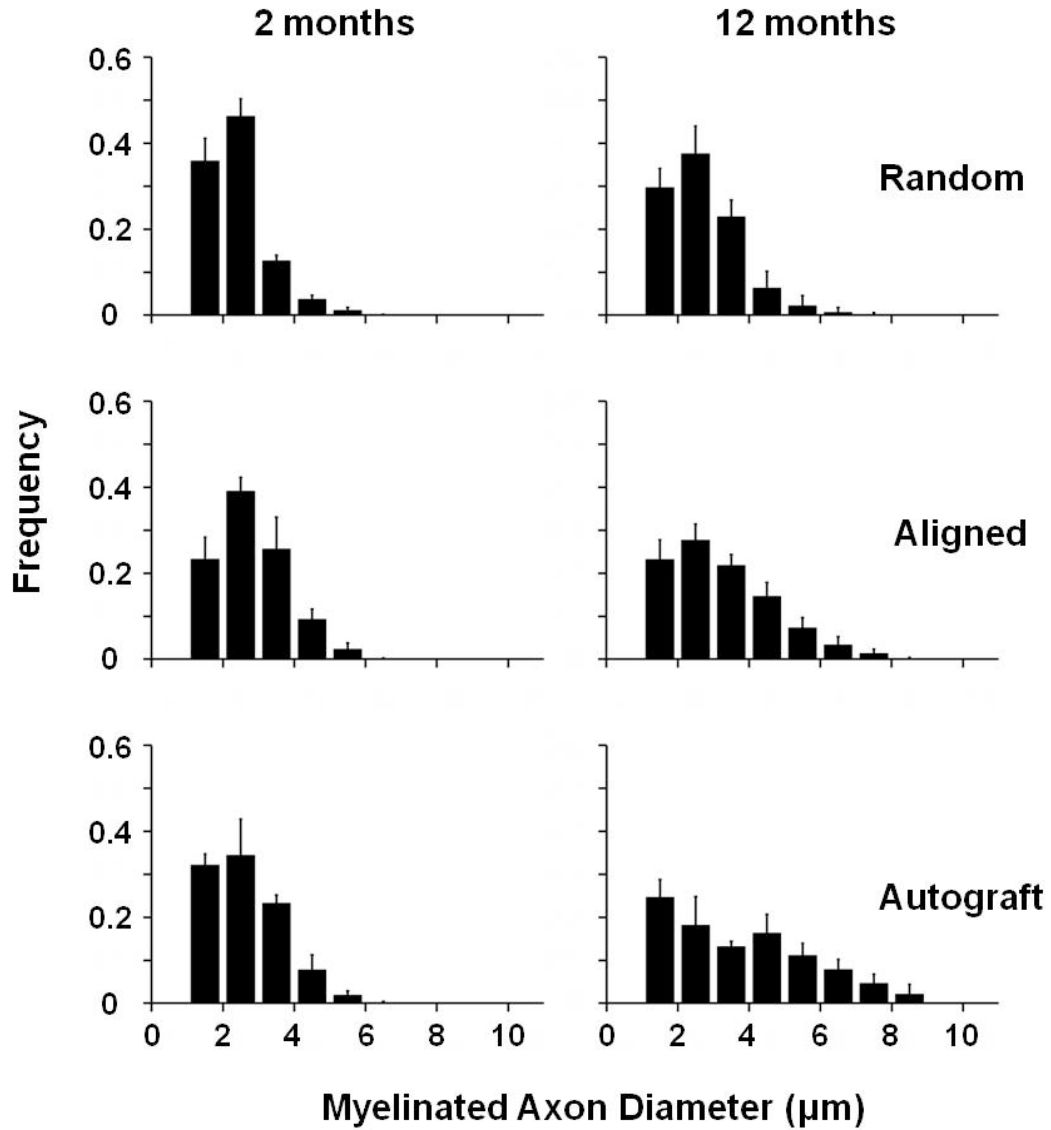
Figure 2.6. Frequency distribution plot of myelinated axon diameter in aligned and random nanofibrous nerve conduit and autograft groups at 2 and 12 months.

nerve conduit group showed similar axon diameter distribution to the autograft group (Figure 2.6.), but the autograft group had more axons with thicker myelin sheaths.

At the 12-month time point, the axon diameter and myelin sheath thickness of the regenerated nerve tissue were significantly increased compared to those at 2 months in all three groups (Figures 2.6., 2.7.), which indicated the further maturation of the
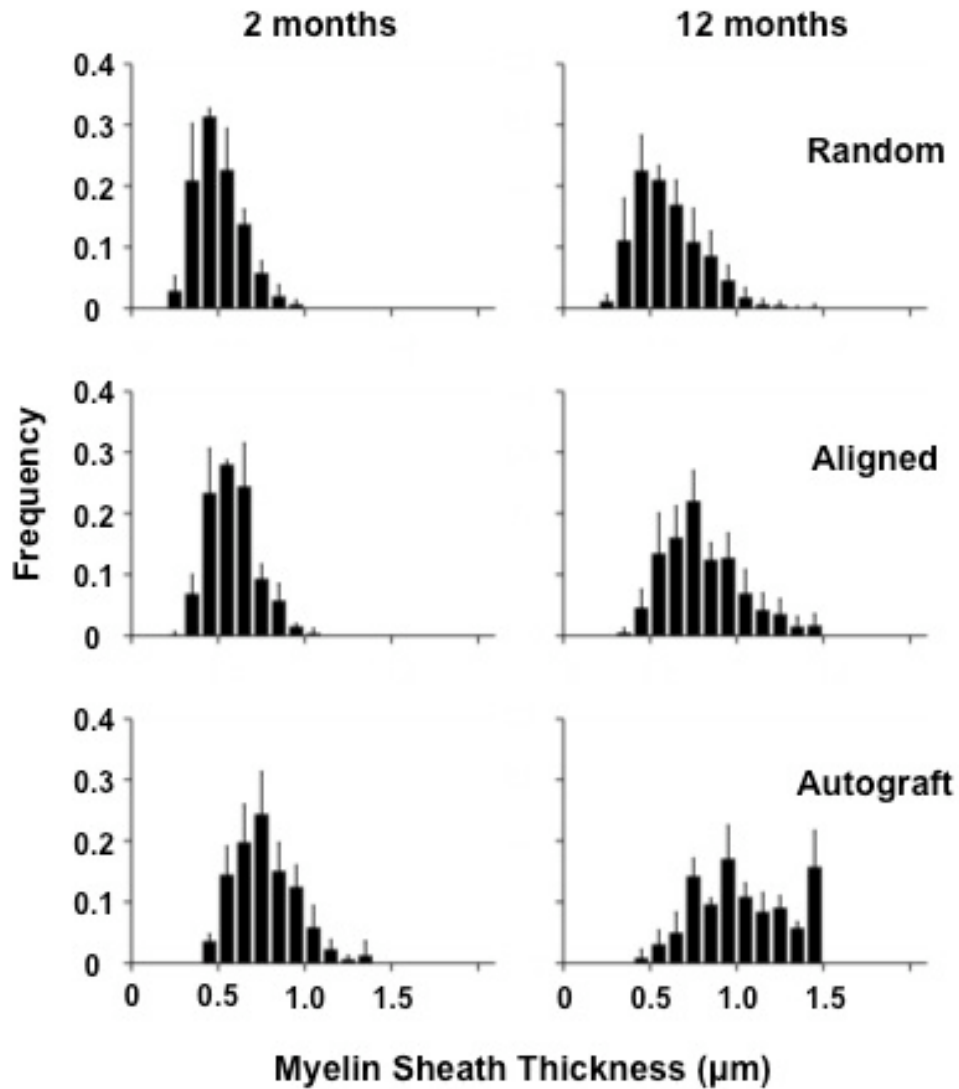
Figure 2.7. Frequency distribution plot of myelin sheath thickness in aligned and random nanofibrous nerve conduit and autograft groups at 2 and 12 months.

regenerated nerves. The aligned nanofibrous nerve conduit group displayed

higher frequencies of large axons (>4 μm in diameter) and thick myelin sheaths (>0.6

μm in thickness) than the random nanofibrous nerve conduit group. The autograft group

had the most axons with thicker (>1.2 μm) myelin sheaths.

2.4. DISCUSSION

Due to the difficulty of electrospinning nerve conduits composed of nanofibers

aligned along the conduit's long axis, researchers in previous studies [19-20] either

rolled a film with aligned nanofibers to form a conduit or filled a silicone tube with aligned

nanofiber sheets. Here we developed a one-step electrospinning process to fabricate a

novel, seamless, tubular nanofibrous nerve conduit composed of two fully-integrated

layers: a luminal layer with longitudinally aligned nanofibers and an outer layer with

randomly organized nanofibers. To our knowledge, this was the first demonstration that a

bi-layer tubular device with longitudinally aligned nanofibers can be directly electrospun

as a unified, seamless construct.

Unlike previous attempts, the device and process described here are much more

amenable and scalable for manufacturing and clinical use. The bi-layer design is likely to

provide better suturability and mechanical integrity than a conduit composed entirely of

longitudinally aligned nanofibers. Mechanical testing and *in vivo* results showed that

this bi-layer nerve conduit has adequate mechanical strength for suturing and for

supporting nerve growth. Direct electrospinning of bi-layer nanofibrous conduits is a fast

process that avoids the tedious and unreliable process of rolling and sealing sheets and

easily adapts to larger conduit sizes and longer lengths. The seamless construction of

the bi-layer nanofibrous conduit also presents a smooth, even luminal surface for nerve

growth and poses no risk of mechanical failure or separation at the seam.

We evaluated the nerve regeneration capacity of bi-layer aligned nanofibrous conduits in a rat sciatic nerve transection model with random nanofibrous conduits and autografts as controls. Nerve regeneration and muscle innervation were assessed at 2-month and 12-month time points with histomorphometry and electrophysiology, respectively.

Electrophysiological analysis demonstrated the superior capability of aligned nanofibrous nerve conduits in nerve regeneration when compared to random nanofibrous nerve conduits. Based on the 2-month results, better functional recovery in terms of CMAP amplitude and conduction velocity was observed in the aligned nanofibrous nerve conduit group than in the random nanofibrous nerve conduit group. Interestingly, the advantage of the autograft was not shown in this early recovery period. One explanation is that that autograft may have to remodel its existing cellular and matrix contents (e.g., degradation and reorganization) to allow the ingrowth of regenerating axons. The 2-month electrosphysiology results suggest that aligned nanofibrous conduits were the most efficient in accelerating nerve functional recovery at the early phase. At the 12-month time point, both aligned nanofibrous nerve conduits and autografts performed significantly better than random nanofibrous nerve conduits, and there was no statistical difference between aligned nanofibrous nerve conduits and autografts. These results indicate that nanofiber organization had long-term effects on nerve regeneration and that the *in vivo* performance of aligned nanofibrous nerve conduits is similar to autografts, which is the current gold standard of treatment for peripheral nerve injuries.

Histological analysis of explanted nerve samples showed myelinated axons, vasculature and epineurial sheaths in both random and aligned nanofibrous nerve conduits at 2 months and 12 months, similar to that in autografts. Quantitative analysis

revealed a higher frequency of large diameter axons and thick myelin sheaths for the aligned nanofibrous nerve conduit group compared to the random nanofibrous nerve conduit group at both time points. Temporal comparison showed obvious shifts toward larger axons and thicker myelin sheaths at 12 months for both the aligned nanofibrous nerve conduit and autograft groups. In contrast, the axon diameter and myelin sheath thickness in the random nanofibrous nerve group at 12 months only showed marginal increase. The axon diameter in aligned nanofibrous conduits and autografts had a similar distribution profile. Interestingly, the myelin sheath was generally thicker in autografts than in aligned nanofibrous conduits. It is possible that pre-existing Schwann cells in autografts played an important role in the myelination of regenerating axons, which may explain the difference in myelination between synthetic grafts and autografts.

The difference in distribution profiles between aligned and random nanofibrous nerve conduits suggests that longitudinally aligned nanofibers accelerate growth of large myelinated axons, which are morphological characteristics of motor neurons. The presence of larger axons with thicker myelin sheaths may also account for the higher CMAP amplitude and faster conduction velocity measured in the aligned nanofibrous nerve conduit group. A major limitation of nerve repair in humans is the slower growth of motor nerve fibers and relatively poor re-innervation of target muscle compared to sensory nerve fiber growth [1,13]. The potential ability of aligned nanofibrous nerve conduits to improve the regeneration of motor nerve fibers and to match the biological performance of autografts merits further study.

Another interesting finding is the difference in the thickness of the fibrous tissue layer on the luminal surface of random and aligned nanofibrous nerve conduits. At 2 months, a thin continuous epineurial-like layer developed at the nerve-conduit interface in both random and aligned nanofibrous nerve conduit groups. At the 12 month time point, a dense connective tissue stroma formed around the regenerated nerve in the

random nanofibrous nerve conduit group, whereas a thin tissue layer resembling a normal epineurium was observed in the aligned nanofibrous conduit group. These results suggest that random and aligned nanofibers not only had different effects in the early phase of nerve regeneration, but also exerted long-term effects during the maturation and remodeling of the regenerated nerve. One possible reason for the differences in epineurial thickness may be due to the differences in roughness between the aligned and random nanofibrous luminal surfaces. The aligned nanofibrous layer provides a smooth uniform surface while the random nanofibrous layer provides a rougher, more uneven surface. Previous studies demonstrated that nerve conduits with rough inner surfaces led to the accumulation of fibroblasts and macrophages and eventually the formation of a fibrous capsule layer around the regenerated nerve [24]. These results may also suggest another advantage of the seamless nanofibrous conduit over nerve conduits with seams or discontinuous luminal surfaces, which may be more susceptible to fibrous capsule formation.

2.5. CONCLUSION

We developed a one-step electrospinning process to demonstrate, for the first time, a seamless nerve conduit with longitudinally aligned nanofibers. The novel nanofibrous conduit has a bi-layer construction: the luminal layer having longitudinally aligned nanofibers to promote nerve regeneration, and the outer layer having randomly organized nanofibers for mechanical support. Long-term *in vivo* studies demonstrated that bi-layer aligned nanofibrous nerve conduits were superior to random nanofibrous conduits and had therapeutic effects comparable to autografts in terms of nerve regeneration and muscle innervation.

2.6. REFERENCES

[1] Belkas JS, Shoichet MS, Midha R. Peripheral nerve regeneration through guidance tubes. Neurol Res. 2004;26:151-60.

[2] Hudson AR, Morris J, Weddell G, Drury A. Peripheral nerve autografts. J Surg Res. 1972;12:267-74.

[3] Martini R. Expression and functional roles of neural cell surface molecules and extracellular matrix components during development and regeneration of peripheral nerves. J Neurocytol. 1994;23:1-28.

[4] Williams LR, Longo FM, Powell HC, Lundborg G, Varon S. Spatial-temporal progress of peripheral nerve regeneration within a silicone chamber: parameters for a bioassay. J Comp Neurol. 1983;218:460-70.

[5] Mackinnon SE, Dellon AL. Clinical nerve reconstruction with a bioabsorbable polyglycolic acid tube. Plast Reconstr Surg. 1990;85:419-24.

[6] Kiyotani T, Teramachi M, Takimoto Y, Nakamura T, Shimizu Y, Endo K. Nerve regeneration across a 25-mm gap bridged by a polyglycolic acid-collagen tube: a histological and electrophysiological evaluation of regenerated nerves. Brain Res. 1996;740:66-74.

[7] Bender MD, Bennett JM, Waddell RL, Doctor JS, Marra KG. Multi-channeled biodegradable polymer/CultiSpher composite nerve guides. Biomaterials. 2004;25:1269-78.

[8] Evans GR, Brandt K, Katz S, Chauvin P, Otto L, Bogle M, et al. Bioactive poly(L-lactic acid) conduits seeded with Schwann cells for peripheral nerve regeneration. Biomaterials. 2002;23:841-8.

[9] Archibald SJ, Shefner J, Krarup C, Madison RD. Monkey median nerve repaired by nerve graft or collagen nerve guide tube. J Neurosci. 1995;15:4109-23.

[10] Wang X, Hu W, Cao Y, Yao J, Wu J, Gu X. Dog sciatic nerve regeneration across a 30-mm defect bridged by a chitosan/PGA artificial nerve graft. Brain. 2005;128:1897-910.

[11] Wang A, Ao Q, Cao W, Yu M, He Q, Kong L, et al. Porous chitosan tubular scaffolds with knitted outer wall and controllable inner structure for nerve tissue engineering. J Biomed Mater Res A. 2006;79:36-46.

[12] Sierpinski P, Garrett J, Ma J, Apel P, Klorig D, Smith T, et al. The use of keratin biomaterials derived from human hair for the promotion of rapid regeneration of peripheral nerves. Biomaterials. 2008;29:118-28.

[13] Schmidt CE, Leach JB. Neural tissue engineering: strategies for repair and regeneration. Annu Rev Biomed Eng. 2003;5:293-347.

[14] Hirono T, Torimitsu K, Kawana A, Fukuda J. Recognition of artificial microstructures by sensory nerve fibers in culture. Brain Res. 1988;446:189-94.

[15] Clark P, Britland S, Connolly P. Growth cone guidance and neuron morphology on micropatterned laminin surfaces. J Cell Sci. 1993;105 (Pt 1):203-12.

[16] Yang F, Murugan R, Wang S, Ramakrishna S. Electrospinning of nano/micro scale poly(L-lactic acid) aligned fibers and their potential in neural tissue engineering. Biomaterials. 2005;26:2603-10.

[17] Patel S, Kurpinski K, Quigley R, Gao H, Hsiao BS, Poo MM, et al. Bioactive nanofibers: synergistic effects of nanotopography and chemical signaling on cell guidance. Nano Lett. 2007;7:2122-8.

[18] Chew SY, Mi R, Hoke A, Leong KW. The effect of the alignment of electrospun fibrous scaffolds on Schwann cell maturation. Biomaterials. 2008;29:653-61.

[19] Chew SY, Mi R, Hoke A, Leong KW. Aligned Protein-Polymer Composite Fibers Enhance Nerve Regeneration: A Potential Tissue-Engineering Platform. Adv Funct Mater. 2007;17:1288-96.

[20] Kim YT, Haftel VK, Kumar S, Bellamkonda RV. The role of aligned polymer fiber-based constructs in the bridging of long peripheral nerve gaps. Biomaterials. 2008;29:3117-27.

[21] Patel S, Diao E, Li S. Aligned Nanofibrous Grafts for Enhanced Nerve Regeneration. 6th Combined Meeting of the Orthopaedic Research Societies. 2007.

[22] Ayres CE, Jha BS, Meredith H, Bowman JR, Bowlin GL, Henderson SC, et al. Measuring fiber alignment in electrospun scaffolds: a user's guide to the 2D fast Fourier transform approach. J Biomater Sci Polym Ed. 2008;19:603-21.

[23] Katayama Y, Montenegro R, Freier T, Midha R, Belkas JS, Shoichet MS. Coil-reinforced hydrogel tubes promote nerve regeneration equivalent to that of nerve autografts. Biomaterials. 2006;27:505-18.

[24] Aebischer P, Guenard V, Valentini RF. The morphology of regenerating peripheral nerves is modulated by the surface microgeometry of polymeric guidance channels. Brain Res. 1990;531:211-8.

Chapter 3.

Nanofibrous Patches for Spinal Cord Regeneration

3.1. INTRODUCTION

Spinal cord injury (SCI) and the resulting chronic paralysis affect more than a million individuals in United States. To date spinal cord regeneration remains as one of the most challenging problems in regenerative medicine, and there is no effective cure for spinal cord injury. The advances in nanotechnology and neuroscience provide new opportunities for us to meet this challenge. The difficulty in axon regeneration in spinal cord is largely due to glial scar formation and the release of inhibitory factors following spinal cord injury [1-5]. Following SCI, the lesion is invaded by fibroblasts, macrophages and glial cells, and a dense glial scar forms. The myelin sheath also degenerates. Both the glial scar and myelin breakdown products become barriers to axon regeneration [6-7]. To overcome this barrier, the stimulation and guidance of axon growth are needed.

Previous studies have suggested that combinations of strategies such as bridging the lesion, drug delivery and cell delivery could result in effective therapies for SCI [8-10]. There is evidence that the inhibitory effects of myelin-derived factors can be eliminated by elevating cAMP activity [11-12]. For example, the inhibition of cAMP hydrolysis by the phosphodiesterase IV inhibitor rolipram (delivered by a mini pump) enhances axon growth in spinal cord [13]. Rolipram also has anti-inflammatory effects in the central nervous system (CNS) [14]. However, how to combine axon guidance and rolipram delivery *in vivo* in a local and sustained manner needs to be addressed.

Several groups have used scaffolds to bridge the gap in the lesion area caused by the necrosis and apoptosis of cells after SCI [15-18]. These scaffolds are either porous solid materials or hydrogels. Recently, electrospinning has been used to fabricate nanofibrous scaffolds from both native matrix and synthetic polymers [19-22]. We have developed nanofibrous scaffolds for tissue regeneration by using electrospinning

technology [23-25]. The aligned nanofibers not only guide axon growth, but also provide a large surface area and can be functionalized by immobilizing bioactive factors [24]. For example, we have shown that aligned nanofibers immobilized with growth factor can synergistically promote axon growth from dorsal root ganglion (DRG) tissue. The prolonged release of bioactive factors by nanofibrous scaffolds can replace the injections or mini-pump administration of bioactive factors at the lesion site.

Here we developed nanofibrous scaffolds that not only guide axon growth and angiogenesis but also release drug locally to promote the regeneration of spinal cord tissue. Rolipram is a selective inhibitor of cyclic AMP phosphodiesterase IV and has antidepressant and anti-inflammatory effects in the central nervous system [26]. By using rolipram as a prototypical drug to augment the response to scaffold support, we showed that rolipram-loaded nanofibrous scaffolds can enhance axon growth and angiogenesis, suppress glial scar formation, and significantly improve the recovery of hindlimb function in the hemisection SCI model.

3.2. MATERIALS AND METHODS

3.2.1. Scaffold Fabrication and Characterization

We used electrospinning technology to fabricate biodegradable scaffolds with a two-layer structure. Poly (L-lactide) PLLA (1.09 dl/g inherent viscosity) and Poly (D, L-lactide-co-glycolide) PLGA (50:50, 0.55~0.75 dl/g inherent viscosity) were from Lactel Absorbable Polymers Inc (Pelham, AL). To make the inner layer with aligned nanofibers, the jet stream of PLLA /PLGA (each 15% weight/volume) solution from the spinneret whipped between the two conductive ends of a plastic mandrel, resulting in aligned nanofibers on the non-conductive portion in the middle of a slowly rotating mandrel. The

outer layer with random nanofibers was generated by increasing the rotating speed of the mandrel to 800 rpm. The scaffold in half-cylindrical shape was made by cutting open the tubular scaffold in the longitudinal direction (Figure 3.1.A). The scaffolds were rinsed with phosphate buffered saline (PBS) and sterilized by UV irradiation before being used for rolipram immobilization or *in vivo* studies. The alignment of nanofibers and the structure of the nanofibrous scaffolds were examined by scanning electron microscopy (SEM). The diameter of nanofibers ranged from 500-800 nm.

3.2.2. Neural Stem Cell (NSC) Interaction with Nanofibrous Scaffolds

Human embryonic stem cells (hESC), line H9 (Wicell, Madison, WI), were cultured as previously described [27]. hESCs were detached with the treatment of 1 mg/mL collagenase, 0.5mg/mL dispase (Invitrogen, Carlsbad, CA) in Knock-out Dulbecco's Modified Eagle Medium (KO-DMEM)/F12 for 20 minutes. The colonies were gently resuspended in B27 media (DMEM/F12 +2% B27 supplement, 1% L-glutamine, 1% non-essential amino acids (Invitrogen) and grown for 5 days in non-adhesive 6-well culture dishes (Nunc, Rochester, NY) to form embryoid bodies (EBs). EBs were then plated onto tissue culture dishes coated with laminin (1 mg/mL) (Invitrogen) and polyorithine (0.1 mg/mL) (Sigma, St. Louis, MO) (mixed in one solution for coating), and grown for 2-3 days in B27 media supplemented with 20ng/mL bFGF (Peprotech, Rocky Hill, NJ) to allow rosette formation. After rosettes formed, the rosettes were manually collected and cultured in suspension in B27 media with bFGF for one day and then seeded onto either aligned or random nanofiber membrane (pre-coated with laminin and polyorithine) in B27 media without bFGF for one week. Samples were fixed and stained with rabbit anti-rat βIII tubulin (1:200 dilution, Sigma) to show the neurite extension (Figure 3.1. D-E).

3.2.3. Immobilization of Rolipram and *In Vitro* Release Profile

To characterize the drug loading capacity of nanofibrous scaffolds *in vitro*, nanofibrous scaffolds were cut into circular membranes (6 mm in diameter and 600 μm in thickness) with biopsy punches, and soaked in rolipram solutions with various concentrations for 12 hours. Then the nanofibrous scaffolds were washed twice with PBS (100 μl each). The soaking solution and the washing solution were collected and combined, and the amount of rolipram was quantified by using high-performance liquid chromatography (HPLC) to deduce the amount of rolipram entrapped and adsorbed within the nanofibrous scaffolds. HPLC was performed by using a RP-18 column and eluent 30-42% acetonitrile/water. Rolipram was detected by UV absorbance at 280 nm. The standard curve of rolipram showed that the peak area obtained from HPLC analysis was linearly correlated with the amount of rolipram in a wide range of concentrations from 5 μg/ml to 500 μg/ ml (R=0.999) (data not shown).

To obtain the release profile of rolipram, nanofibrous scaffolds were immersed into rolipram solution (500 μg/ml) for 12 hours. The scaffolds were then rinsed twice with PBS, completely submerged in 3 ml PBS solution and incubated at 37ºC for up to 20 days. At selected time points (0.5 hr, 4 hr, 1 day, 2 days, 4 days, 8 days, 12 days, 20 days), 0.3 ml of solution was withdrawn and replaced by 0.3 ml of fresh PBS. The amount of rolipram in the withdrawn solution was determined by HPLC, and the total amount of released rolipram was calculated to generate the release profile.

3.2.4. Spinal Cord Hemisection

All procedures in animal studies were approved by the Institutional Review Board Service and Institutional Animal Care and Use Committee at the University of California,

Berkeley. Male adult athymic rats (250 ± 30 g; 8-week old) were anesthetized with 1.5% isoflurane in 70% N_2O/30% O_2. Body temperature was maintained at 37.0±0.5°C. SCI was performed as described before [11,15,28]. Briefly, the rat was set in the prone position, and the 9th to 11th thoracic vertebrae were exposed. After resecting the laminae, the spinal dura mater was incised to expose the spinal cord. A lateral hemisection at the T9-T11 level was made by creating a 4-mm long longitudinal cut along the midline of the cord, followed by lateral cuts at the rostral and caudal ends and the removal of the tissue by aspiration. Right after SCI, a scaffold (4-mm long, half of a tube with the diameter fitting in the cavity of the injured spinal cord and nanofibers aligned in longitudinal direction) with or without rolipram was used to cover the spinal cord surface and enclose the lesion site. The scaffold was thick enough (~600 µm) to separate spinal cord from surrounding tissue. Fibrin glue was used to glue the outside of the scaffolds to the vertebra tissue as needed. The surgery site was closed in layers. After surgery, rats were kept on heating pads, and daily examination was performed. Abdomen massage was done to help evacuate urine from the bladder as needed.

3.2.5. Immunohistochemistry

Frozen sections (10 µm in thickness) of spinal cord tissues were fan-dried for 1 hour at room temperature. Then the slides were fixed in 4% paraformaldehyde solution for 25 minutes at room temperature. Samples were incubated in 5% normal goat serum for 30 minutes to block non-specific binding, and then incubated with primary antibody diluted in 5% normal goat serum overnight at 4°C. Primary antibodies include mouse anti-CD31 (1:100 dilution, BD Pharmigen) for endothelial cells (ECs), rabbit anti-neurofilament (1:200 dilution, Sigma) for axons, mouse anti-glial fibrillary acidic protein (GFAP) (1:2000 dilution, Sigma) for astrocytes, anti-chondroitin sulfate proteoglycans

(CSPGs) (1:200 dilution, Millipore, Billerica, MA) for glial scars. Negative controls were included by omitting the primary antibody. The sections were incubated for one hour with either horseradish peroxidase-conjugated anti-mouse or rabbit IgG (1:1000, Alexa 594 for red and Alexa 488 for green, Invitrogen, Carlsbad, CA). Finally, slides were mounted and examined by using a fluorescence microscope (Zeiss Axioskop 2 MOT).

3.2.6. Hindlimb Behavioral Assessment

Three groups in this study were investigated to evaluate functional recovery after SCI by hindlimb behavioral assessment. Animals that had undergone SCI without any treatments were considered as the untreated group and experimental groups included scaffold only and scaffold plus rolipram groups. One day after SCI, and subsequently every other week, Basso-Beattie-Bresnahan (BBB) locomotor scale rating was performed to evaluate the functional recovery of the disabled limb [29]. The BBB locomotor rating scale is an open-field 21-point evaluation scale, with 21 points as the highest score (normal) and 0 as the lowest score (completely disabled). BBB scores were used to categorize the combinations of rat hindlimb movements, trunk stability, stepping, coordination, paw placement, toe drag and tail position. Briefly, BBB score rating was assessed by an observer blinded to the treatment every week. Animals were allowed to move freely in an open area and the movements of hindlimbs were examined and recorded for at least five minutes. A digital camcorder was used to record the movement of rats and replayed in slow motion as needed.

3.2.7. Statistical Analysis

The data are presented as mean ± standard deviation (SD). Data were analyzed using analysis of variance (Statview 5.0) to examine BBB scores. Post hoc testing was

performed by using Fisher's protected least significant difference (PLSD). A P value less than 0.05 was considered statistically significant.

3.3. RESULTS

3.3.1. Structure and Appearance of Nanofibrous Scaffolds

We used electrospinning technology to make a tubular scaffold with longitudinally aligned nanofibers as the inner layer. Layers of random nanofibers were generated outside of aligned nanofibers (Figure 3.1.). The purpose of aligned fibers in the inner
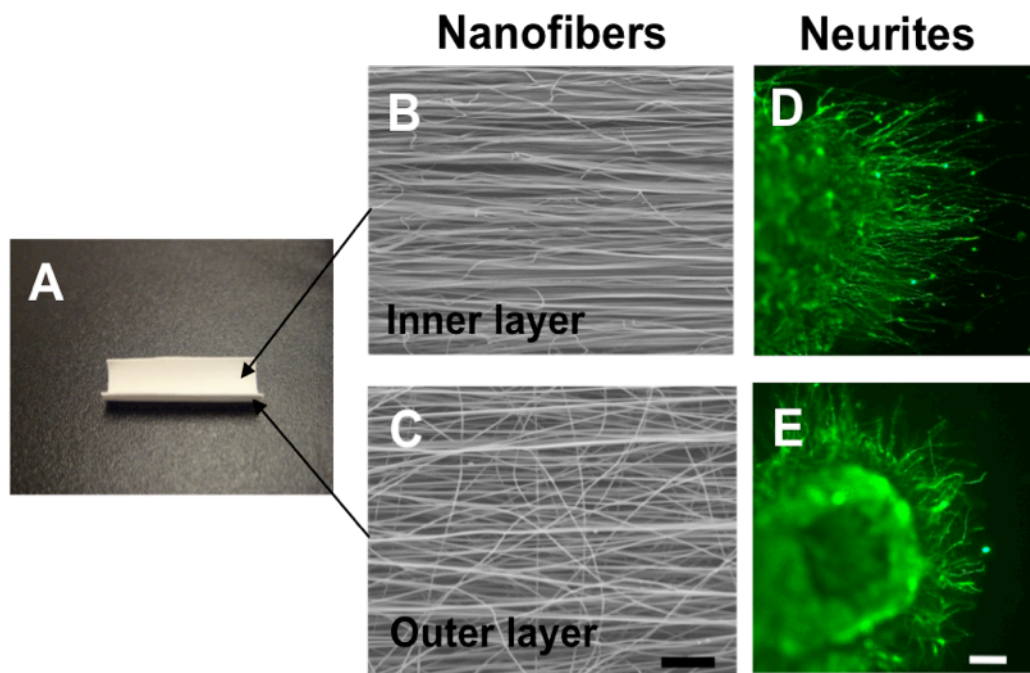
Figure 3.1. Characterization of nanofibrous scaffolds with both aligned and random layers. (A) The scaffold in half-cylindrical shape was made from a tubular scaffold and cut open in the longitudinal direction. SEM images showed the inner layer (B) with longitudinal aligned fibers and outer layer (C) with random fibers of the scaffold. Scale bar = 20 μm. Human ESC derived neural cells cultured on aligned (D) and random (E) nanofiber surfaces *in vitro* for one week in B27 media. Neurites were stained by βIII-tubulin antibody. Scale bar = 100 μm.

layer (~100 µm in thickness) was to provide guidance for the growth of axons in the longitudinal direction of spinal cord and facilitate axon growth into the three-dimensional (3D) scaffold, and the outer layer (~500 µm in thickness) with random nanofibers enhanced the mechanical property of the scaffolds.

3.3.2. Aligned Nanofibers Promote Neurite Growth from NSCs

To characterize the role of nanofibrous scaffolds on neurite growth, we seeded NSCs onto scaffolds with either aligned or random nanofibers. As shown in Figure 3.1., aligned nanofibrous scaffolds guide neurite growth from rosettes in the direction of nanofiber alignment (Figure 3.1.D), but neurites extended randomly on the surface of random nanofibers (Figure 3.1.E).

3.3.3. Immobilization of Rolipram onto Nanofibrous Scaffolds

As shown in Figure 3.2.A, the amount of rolipram entrapped/adsorbed within the nanofibrous scaffolds increased with the input rolipram solution concentration, and reached a plateau beyond input concentrations of 250 µg/ml. The *in vitro* rolipram release profile is shown in Figure 3.2.B. The results showed that drug release occurred in three phases: a first initial burst release, a fast release of the drug over the first 3 days, and a sustained and slow release of the drug over 20 days.
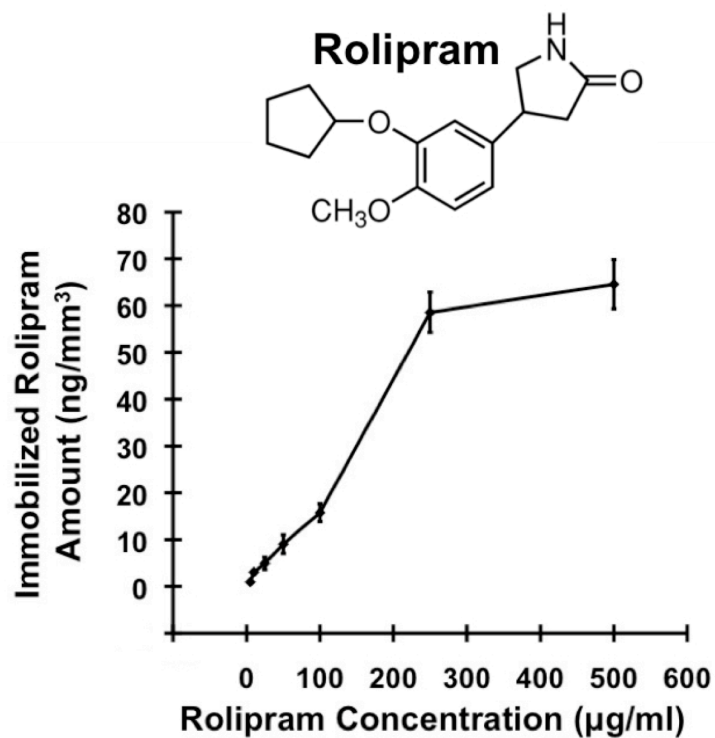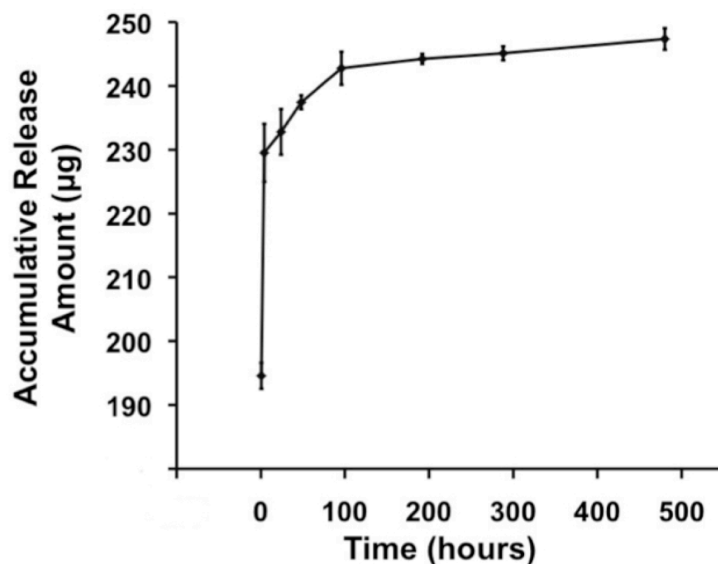
Figure 3.2. *In vitro* immobilization and release profile of rolipram with nanofibrous scaffolds by performing the HPLC test. (A) The amount of rolipram immobilized within the nanofibrous scaffolds with different rolipram loading concentrations. (B) The release profile of rolipram in PBS at 37°C.

3.3.4. Nanofibrous Scaffolds with Rolipram Enhanced Axon Growth,

Increased Angiogenesis and Decreased Glial Scar

To test the therapeutic effects of rolipram-loaded nanofibrous scaffolds, rats were subjected to T9-11 spinal cord hemisection as the SCI model. Right after the injury, the lesion was either left untreated (control group), or bridged with nanofibrous scaffolds with or without immobilized rolipram (Figure 3.3.)
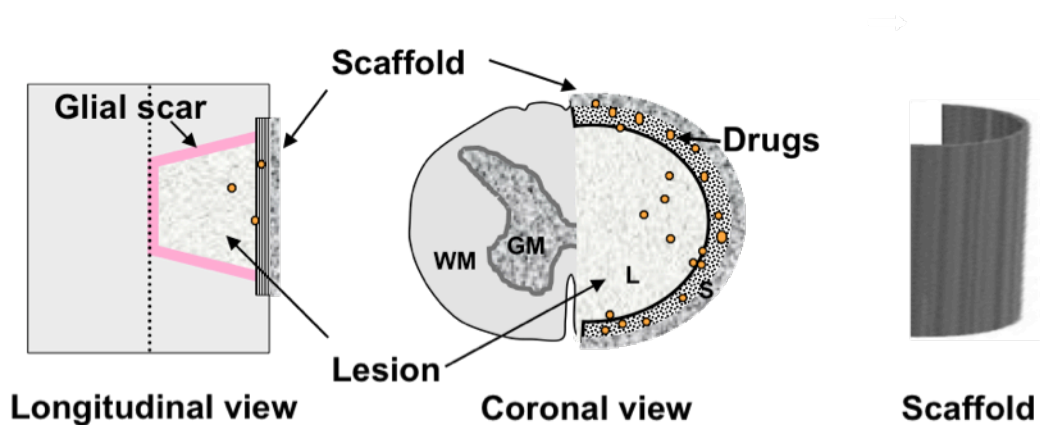
Figure 3.3. Schematic illustration of our approach to promote spinal cord regeneration. Scaffolds with nanofibers (in the inner layer) aligned in the longitudinal direction were used to bridge the lesion, guide axons and deliver rolipram locally.

After 12 weeks, three rats in each group were sacrificed, and the cross sections of the spinal cord tissues were used for histological analysis. The histological staining of samples from three groups (untreated control, scaffold and scaffold with rolipram) is shown in Figure 3.4. and 3.5.. As an example, H&E staining of a cross section from the scaffold with rolipram group (Figure 3.4.A) showed the intact white and grey matter on the left side of the spinal cord and the lesion area on the right side with some loose

regenerated tissue. Black dashed lines sketch the boundary between the lesion and
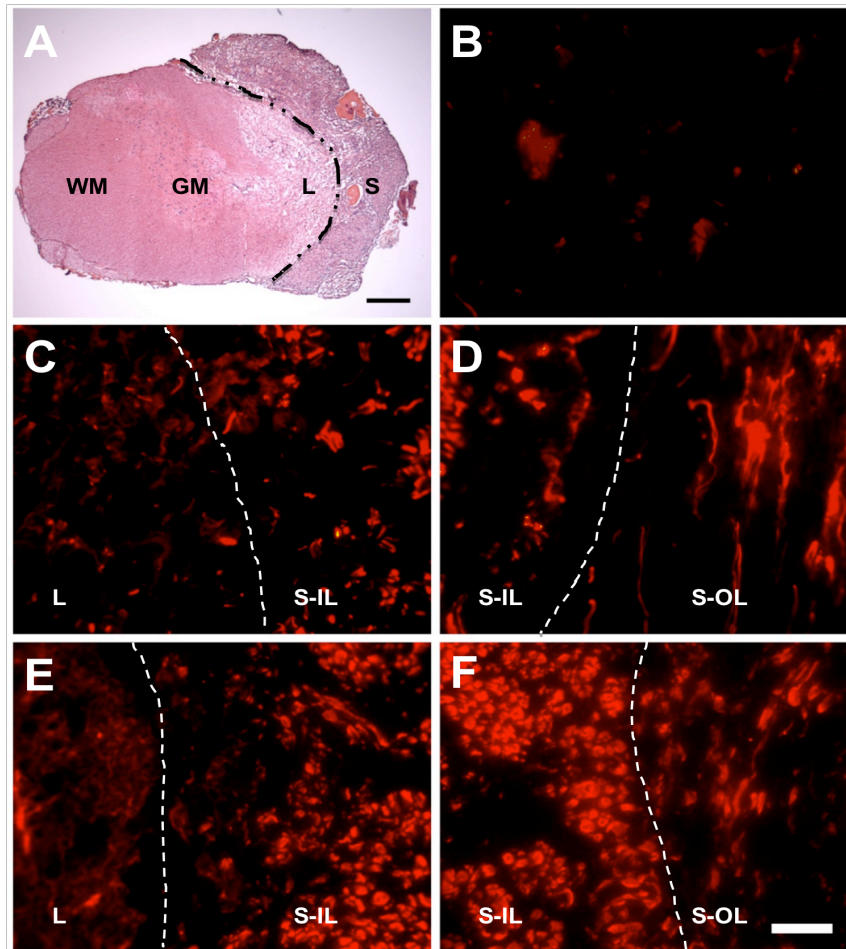
scaffold.

Figure 3.4. H&E staining and neurofilament staining after 12 weeks of spinal cord hemisection surgery. (A) H&E staining showed an injury lesion after 12 weeks of SCI in the group with scaffolds plus rolipram. Black dashed lines show the boundary between the lesion and scaffold. Scale bar =500 mm. (B-F) Immunofluorescent staining of cross sections showed neurofilament staining of axons in the area of damaged white matter and scaffold in the untreated (B), scaffold (C,D) and scaffold with rolipram (E,F) groups. White dashed lines show the boundary either between the lesion and inner layer of scaffold (C,E) or between the inner layer and outer layer of scaffold (D,F). Scale bar = 20 mm. Abbreviations are: WM, white matter; GM, grey matter; L, lesion; S, scaffold; S-IL, scaffold-inner layer; S-OL, scaffold-outer layer.

Neurofilaments are major elements of the cytoskeleton in the axon cytoplasm, which were immunostained to show neurons and axon growth in the tissue. The scaffolds with or without rolipram increased axon growth through the scaffolds and in the lesion, with the most axon growth in the inner layer of the scaffolds with rolipram (Figure 3.4.C-F). In addition, axon growth showed different directions in the longitudinal aligned and random nanofibrous layers, suggesting the primary role of nanofibers in the guidance of axon regeneration.
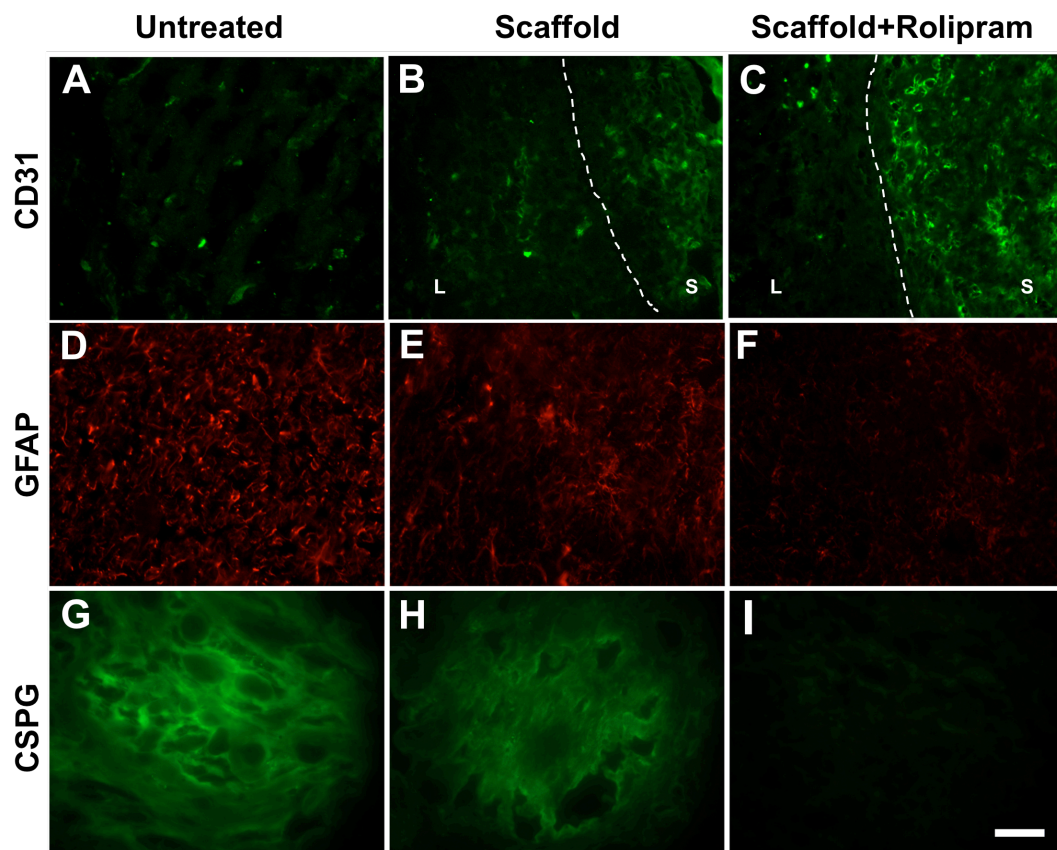
Figure 3.5. Histological analysis of CD31, GFAP and CSPG staining after 12 weeks of spinal cord hemisection surgery. Immunofluorescent staining of cross sections (in the area of damaged white matter around the longitudinal middle section of the lesion and near the scaffolds) from untreated lesions (A,D,G), lesions treated with scaffold alone (B,E,H) and lesions treated with scaffold plus rolipram (C,F,I). ECs in capillaries were stained by CD31 antibody (A-C). White dashed lines show the boundary between the lesion (L) and scaffold (S). Astrocytes in the lesion were stained for GFAP antibody (D-F). Glial scars were stained for CSPG antibody (G-I). Scale bar = 20 μm.

Moreover, positive CD31 staining for ECs was found in nanofibrous scaffolds. Angiogenesis through the scaffold was detected in the scaffold alone group (Figure 3.5.B), suggesting that the aligned nanofibers guided EC migration. Interestingly, the combination of nanofibrous scaffold and rolipram further promoted angiogenesis through the scaffold (Figure 3.5.C).

Furthermore, the least GFAP staining was found in the lesion treated with scaffolds plus rolipram, which correlated well with the lowest CSPGs expression (Figure 3.5.F and Figure 3.5.I), suggesting that rolipram could reduce the number of reactive astrocytes and suppress inflammatory responses and glial scar formation.
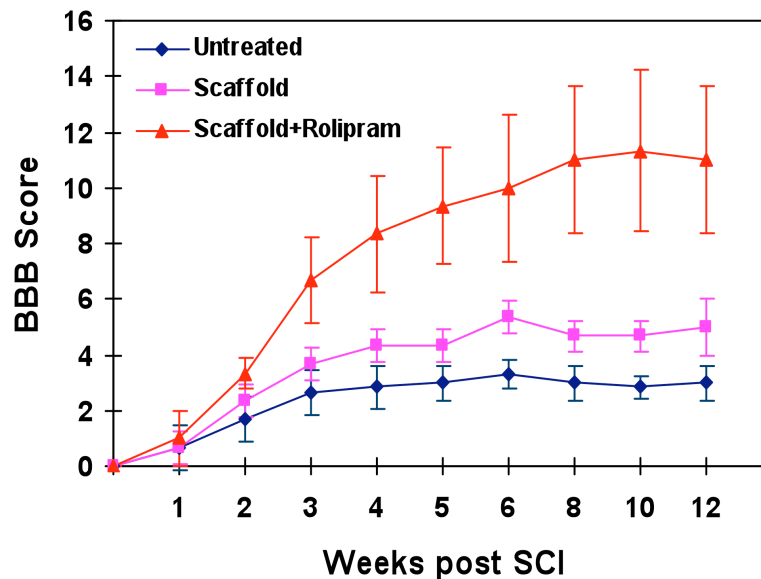
Figure 3.6. Functional recovery of hindlimb locomotion as indicated by BBB score. After spinal cord hemisection, hindlimb locomotor function was analyzed every week throughout 12-week survival time periods. * indicates significant difference (P<0.05) compared to the control group at the respective time points. Three animals were used in each group.

3.3.5. Release of Rolipram from Nanofibrous Scaffolds Promote Functional Recovery

To determine whether the insertion of nanofibrous scaffold with or without rolipram promoted the recovery of hindlimb motor function, behavioral analysis was performed by using the BBB locomotor scale rating. As shown in Figure 3.6., scaffold alone only had a modest effect on functional recovery after 6 weeks. Rolipram plus scaffold significantly improved hindlimb function after 3 weeks. During weeks 3-8, the BBB score of hindlimb movement increased at every observation point in the group with scaffold plus rolipram. After 8 weeks, the hindlimb function had no further improvement in all three groups.

3.4. DISCUSSION

The difficulty in spinal cord regeneration can be attributed to multiple factors, including the limited regeneration capability of neurons in the CNS, the lack of appropriate axon guidance in the lesion, and the inhibitory factors such as myelin breakdown products and CSPGs in glial scars. Most efforts to restore function after spinal injury have been directed toward enhancing damaged axons to regenerate through the injury site, and then reconnecting the proper targets to restore motor and sensory function. Here we developed a biodegradable nanofibrous scaffold with immobilized rolipram to facilitate spinal cord tissue regeneration.

Nanostructured materials have tremendous potential for tissue engineering. Our results showed that aligned nanofibers guided neurite growth *in vitro* (Figure 3.1.). In addition, axon growth in the inner and outer layers of the scaffolds show different directions following nanofibers (Figure 3.4.C-F), indicating that aligned nanofibers can guide axon growth *in vivo*. Furthermore, aligned nanofibers could also promote axon

growth and cell infiltration [25] into the 3D scaffolds. The release of rolipram from the nanofibers significantly increased axon growth through the inner layer of the scaffolds (Figure 3.4.E-F), suggesting a synergistic effect of aligned nanofibers and drug release, which is well correlated with the behavior test results (Figure 3.6.). The modest functional recovery in the scaffold group suggests that axon guidance alone is not sufficient, but it is likely that aligned nanofibers are necessary to achieve the functional recovery—otherwise axon growth may be disorganized and cannot reach the target area effectively. Whether random nanofibrous scaffolds with rolipram could promote functional recovery awaits further study.

In addition to promoting axon growth, the therapeutic effects of rolipram could also be attributed to the suppression of inflammatory responses and glial scar formation, as shown by the decrease of CSPGs and glial cells in the lesion area (Figure 3.5.D-I). CSPGs are a major component of glial scars synthesized by glial cells and inflammatory cells, which form a physical and biochemical barrier to axon growth [30-31]. Rolipram can elevate cAMP acitivity, thus suppressing inflammatory effects and inhibiting reactive astrocyte related astrogliosis [32-33]. Generally, rolipram at high doses can be used as an inflammatory drug, which prevents secondary cell loss in the acute stage [26,34]. Acute rolipram treatment retards the injury-induced increase of IL-1β and TNF-α, which are prominently elevated at the lesion and cause secondary tissue degeneration [35]. Moreover, recent evidence suggests that rolipram modulates pro-apoptotic caspase-3 activity to provide neuroprotection against several apoptotic insults [36].

Our rolipram release profile is well suited to address the need to suppress inflammatory responses at the early stage and promote axon growth at the later stage. Rolipram is a small hydrophobic molecule with a three-ring structure. Here rolipram was adsorbed onto hydrophobic PLLA/PLGA nanofibers, potentially through hydrophobic interactions through multiple sites on the molecule. The exact binding sites have not

been mapped out. We found that most rolipram was released in the first day, and then the nanofibrous scaffold continuously released lower levels of rolipram into the solution continuously for 20 days. The instant release of 90% of rolipram from the nanofibrous scaffold may play a major role in attenuating early inflammation. Following the initial burst of rolipram release, the low dose of rolipram release might be effective in stimulating axon growth. Previous investigation showed that increasing cAMP levels in neurons enhanced the responsiveness to diffusible growth factor and overcame myelin-associated inhibitory molecules to promote axonal growth and neuritis [37]. Further investigations will be conducted to engineer the drug loading capacity and release profile and to determine the differential effects of rolipram at the early and late stages of the spinal cord repair. It should also be noted that the athymic rats used in this study have T-cell deficiency, and possible immunological responses involving T cells are not included in this animal model.

Interestingly, in addition to axon growth into the scaffolds, extensive angiogenesis was detected in the scaffold, which was further enhanced by rolipram treatment. The mechanisms are not clear and need further investigation. Recent investigation reported that axon regrowth was stimulated by new blood vessel formation in the damaged tissue after spinal cord injury [38] and that vascular endothelial growth factor (VEGF) induced posttraumatic angiogenesis to improve functional recovery of injured rodents [39]. Whether and how angiogenesis in the scaffold contributes to spinal cord regeneration need further investigation.

Overall, this study has demonstrated that nanofibrous scaffolds offered a valuable platform of drug delivery for spinal cord regeneration in addition to the guidance of axon growth and angiogenesis, and that scaffold-mediated rolipram release not only promotes axon growth and angiogenesis but also suppresses glial scar formation.

3.5. REFERENCES

[1] GrandPre T, Nakamura F, Vartanian T, Strittmatter SM. Identification of the Nogo inhibitor of axon regeneration as a Reticulon protein. Nature. 2000;403:439-44.

[2] Mukhopadhyay G, Doherty P, Walsh FS, Crocker PR, Filbin MT. A novel role for myelin-associated glycoprotein as an inhibitor of axonal regeneration. Neuron. 1994;13:757-67.

[3] Niederost BP, Zimmermann DR, Schwab ME, Bandtlow CE. Bovine CNS myelin contains neurite growth-inhibitory activity associated with chondroitin sulfate proteoglycans. J Neurosci. 1999;19:8979-89.

[4] Smith-Thomas LC, Stevens J, Fok-Seang J, Faissner A, Rogers JH, Fawcett JW. Increased axon regeneration in astrocytes grown in the presence of proteoglycan synthesis inhibitors. J Cell Sci. 1995;108 (Pt 3):1307-15.

[5] Schwab ME. Repairing the injured spinal cord. Science. 2002;295:1029-31.

[6] Yiu G, He Z. Glial inhibition of CNS axon regeneration. Nat Rev Neurosci. 2006;7:617-27.

[7] Fitch MT, Silver J. CNS injury, glial scars, and inflammation: Inhibitory extracellular matrices and regeneration failure. Exp Neurol. 2008;209:294-301.

[8] Baptiste DC, Fehlings MG. Emerging drugs for spinal cord injury. Expert Opin Emerg Drugs. 2008;13:63-80.

[9] Bunge MB. Bridging areas of injury in the spinal cord. Neuroscientist. 2001;7:325-39.

[10] Rowland JW, Hawryluk GW, Kwon B, Fehlings MG. Current status of acute spinal cord injury pathophysiology and emerging therapies: promise on the horizon. Neurosurg Focus. 2008;25:E2.

[11] Neumann S, Bradke F, Tessier-Lavigne M, Basbaum AI. Regeneration of sensory axons within the injured spinal cord induced by intraganglionic cAMP elevation. Neuron.

2002;34:885-93.

[12] Song H, Ming G, He Z, Lehmann M, McKerracher L, Tessier-Lavigne M, et al. Conversion of neuronal growth cone responses from repulsion to attraction by cyclic nucleotides. Science. 1998;281:1515-8.

[13] Nikulina E, Tidwell JL, Dai HN, Bregman BS, Filbin MT. The phosphodiesterase inhibitor rolipram delivered after a spinal cord lesion promotes axonal regeneration and functional recovery. Proc Natl Acad Sci U S A. 2004;101:8786-90.

[14] Zhu J, Mix E, Winblad B. The antidepressant and antiinflammatory effects of rolipram in the central nervous system. CNS Drug Rev. 2001;7:387-98.

[15] Teng YD, Lavik EB, Qu X, Park KI, Ourednik J, Zurakowski D, et al. Functional recovery following traumatic spinal cord injury mediated by a unique polymer scaffold seeded with neural stem cells. Proc Natl Acad Sci U S A. 2002;99:3024-9.

[16] Tysseling-Mattiace VM, Sahni V, Niece KL, Birch D, Czeisler C, Fehlings MG, et al. Self-assembling nanofibers inhibit glial scar formation and promote axon elongation after spinal cord injury. J Neurosci. 2008;28:3814-23.

[17] Oudega M, Gautier SE, Chapon P, Fragoso M, Bates ML, Parel JM, et al. Axonal regeneration into Schwann cell grafts within resorbable poly(alpha-hydroxyacid) guidance channels in the adult rat spinal cord. Biomaterials. 2001;22:1125-36.

[18] Friedman JA, Windebank AJ, Moore MJ, Spinner RJ, Currier BL, Yaszemski MJ. Biodegradable polymer grafts for surgical repair of the injured spinal cord. Neurosurgery. 2002;51:742-51; discussion 51-2.

[19] Liang D, Hsiao BS, Chu B. Functional electrospun nanofibrous scaffolds for biomedical applications. Adv Drug Deliv Rev. 2007;59:1392-412.

[20] Sill TJ, von Recum HA. Electrospinning: applications in drug delivery and tissue engineering. Biomaterials. 2008;29:1989-2006.

[21] Li D, Xia Y. Welding and patterning in a flash. Nat Mater. 2004;3:753-4.

[22] Boland ED, Matthews JA, Pawlowski KJ, Simpson DG, Wnek GE, Bowlin GL. Electrospinning collagen and elastin: preliminary vascular tissue engineering. Front Biosci. 2004;9:1422-32.

[23] Huang NF, Patel S, Thakar RG, Wu J, Hsiao BS, Chu B, et al. Myotube assembly on nanofibrous and micropatterned polymers. Nano Lett. 2006;6:537-42.

[24] Patel S, Kurpinski K, Quigley R, Gao H, Hsiao BS, Poo MM, et al. Bioactive nanofibers: synergistic effects of nanotopography and chemical signaling on cell guidance. Nano Lett. 2007;7:2122-8.

[25] Hashi CK, Zhu Y, Yang GY, Young WL, Hsiao BS, Wang K, et al. Antithrombogenic property of bone marrow mesenchymal stem cells in nanofibrous vascular grafts. Proc Natl Acad Sci U S A. 2007;104:11915-20.

[26] Griswold DE, Webb EF, Breton J, White JR, Marshall PJ, Torphy TJ. Effect of selective phosphodiesterase type IV inhibitor, rolipram, on fluid and cellular phases of inflammatory response. Inflammation. 1993;17:333-44.

[27] Lam H, Patel S, Wong J, Chu J, Lau A, Li S. Localized decrease of beta-catenin contributes to the differentiation of human embryonic stem cells. Biochem Biophys Res Commun. 2008;372:601-6.

[28] He Z, Koprivica V. The Nogo signaling pathway for regeneration block. Annu Rev Neurosci. 2004;27:341-68.

[29] Basso DM, Beattie MS, Bresnahan JC. A sensitive and reliable locomotor rating scale for open field testing in rats. J Neurotrauma. 1995;12:1-21.

[30] Jones LL, Yamaguchi Y, Stallcup WB, Tuszynski MH. NG2 is a major chondroitin sulfate proteoglycan produced after spinal cord injury and is expressed by macrophages and oligodendrocyte progenitors. J Neurosci. 2002;22:2792-803.

[31] Jones LL, Sajed D, Tuszynski MH. Axonal regeneration through regions of chondroitin sulfate proteoglycan deposition after spinal cord injury: a balance of

permissiveness and inhibition. J Neurosci. 2003;23:9276-88.

[32] McKeon RJ, Schreiber RC, Rudge JS, Silver J. Reduction of neurite outgrowth in a model of glial scarring following CNS injury is correlated with the expression of inhibitory molecules on reactive astrocytes. J Neurosci. 1991;11:3398-411.

[33] Chaudhry N, Filbin MT. Myelin-associated inhibitory signaling and strategies to overcome inhibition. J Cereb Blood Flow Metab. 2007;27:1096-107.

[34] Keane RW, Davis AR, Dietrich WD. Inflammatory and apoptotic signaling after spinal cord injury. J Neurotrauma. 2006;23:335-44.

[35] Koopmans GC, Deumens R, Buss A, Geoghegan L, Myint AM, Honig WH, et al. Acute rolipram/thalidomide treatment improves tissue sparing and locomotion after experimental spinal cord injury. Exp Neurol. 2009.

[36] Chen RW, Williams AJ, Liao Z, Yao C, Tortella FC, Dave JR. Broad spectrum neuroprotection profile of phosphodiesterase inhibitors as related to modulation of cell-cycle elements and caspase-3 activation. Neurosci Lett. 2007;418:165-9.

[37] Domeniconi M, Filbin MT. Overcoming inhibitors in myelin to promote axonal regeneration. J Neurol Sci. 2005;233:43-7.

[38] Dray C, Rougon G, Debarbieux F. Quantitative analysis by in vivo imaging of the dynamics of vascular and axonal networks in injured mouse spinal cord. Proc Natl Acad Sci U S A. 2009;106:9459-64.

[39] Widenfalk J, Lipson A, Jubran M, Hofstetter C, Ebendal T, Cao Y, et al. Vascular endothelial growth factor improves functional outcome and decreases secondary degeneration in experimental spinal cord contusion injury. Neuroscience. 2003;120:951-60.

Chapter 4.

iPSC-Derived Neural Crest Stem Cell

Differentiation in Nanofibrous Vascular Scaffolds

4.1. INTRODUCTION

Cardiovascular disease is the leading cause of death in the United States, and every year more than 500,000 coronary artery bypass procedures are performed to cure vascular dysfunctions. However, arterial and venous grafts are limited by their availability and additional surgery/cost, while synthetic vascular scaffolds are limited to large-diameter (>5 mm) grafts due to frequent thrombosis and occlusion. A tissue engineering approach to construct small-diameter scaffolds could be an ideal solution to overcome these limitations.

Native blood vessels have three distinct layers: an anti-thrombogenic endothelial cell (EC) monolayer, a medial layer that is mainly populated by aligned smooth muscle cells (SMCs) embedded in a three-dimensional ECM (mainly collagens and elastin), and an adventitial layer of connective tissue. SMCs and ECs, in combination with ECM or polymers, have been used to fabricate tissue-engineered vascular grafts (TEVGs) [1-3]. Although significant progress has been made, reliable and expandable cell sources, especially non-immunogenic cell sources, for the construction of vascular grafts have not been established, and optimal scaffolds need to be explored as well.

Nanostructured materials have tremendous potential for tissue engineering. Electrospinning technology can be used to generate nanofibrous scaffolds based on synthetic polymers as well as native matrix. Electrospinning is based on the principle that the surface tension associated with a single droplet can be overcome with an applied electric field, thereby creating a Taylor cone and drawing the droplet into a stream in the direction of the field [4-5]. In the past few years, there has been a significant growth of research to explore the applications of electrospun nanofibers. The use of electrospinning to generate functional nanofibrous scaffolds for tissue regeneration is particularly exciting as the structure and morphology of electrospun

scaffolds can be manipulated to resemble that of extracellular matrix (ECM), therefore creating a more "familiar" environment for the cells. Synthetic polymer scaffolds such as those composed of lactic or glycolic acids are biocompatible, have configurable mechanical properties and can be easily modified to incorporate peptides. Recent studies have shown that electrospun nanofibers of polymers and matrix proteins allow the adhesion, proliferation and organized assembly of cells *in vitro* [6-8]. Previous studies have shown that biodegradable nanofibrous vascular scaffolds with bone marrow mesenchymal stem cells (MSCs) allowed excellent extracellular matrix (ECM) remodeling and cell infiltration and organization [9]. Thus, the nanofibrous scaffold could be applied as a model to investigate the remodeling of vascular grafts *in vivo*.

The recent prominent discovery of induced pluripotent stem cells (iPSCs), which are reprogrammed from adult somatic cells, has shown promise for use in the field of regenerative medicine [10-12]. iPSCs are capable of differentiating into various cell types, including neural lineages (peripheral neurons and Schwann cells) [13], mesenchymal lineages (smooth muscles, osteoblasts, chondrocytes, and adipocytes) [12], hematopoietic precursors [14] and hepatocytes [15]. Here we generated human NCSCs from iPSCs as an alternative cell source to mesenchymal stem cells (MSCs) for vascular scaffold application. NCSCs derived from human embryonic stem cells (ESCs) propagated in vitro and were directed toward multiple neural crest lineages [16]. Despite the NCSC's capacity to differentiate, the *in vivo* differentiation of NCSCs in the vascular niche has yet to be explored.

In this study, we developed a one-step procedure to fabricate a seamless vascular scaffold with a bi-layer structure similar to native artery: the luminal surface has longitudinally aligned nanofibers for endothelial cell migration, and the outer layer has circumferentially aligned nanofibers for smooth muscle cell organization and structural support. iPSC-derived NCSCs' differentiation in various matrix stiffness conditions

73

demonstrated the potential of combining iPSCs and nanofibrous scaffolds for vascular tissue engineering. The unique design of matrigel and collagen cellular vascular scaffolds sustained efficient cell recruitment and organization, significant synthesis and self-assembly of ECM, and excellent patency. Moreover, collagen-cellular vascular scaffold with TGF-β showed significant synthesis, self-assembly of ECM and increased mechanical strength. In this chapter, we evaluate the mechanical properties of acellular and cellular vascular scaffolds.

4.2. MATERIALS AND METHODS

4.2.1. Human iPSC-derived NCSC Culture

Undifferentiated human iPSCs (passages 22-45) were maintained as described previously [17]. Briefly, cells were co-cultured with mitotically inactivated mouse embryonic fibroblasts (MEFs) in Knockout DMEM/F-12 medium supplemented with Knockout serum replacer (KSR), 1% non-essential amino acids (NEAA), 1 mM L-glutamine (all from Invitrogen), 0.1 mM ß-mercaptoethanol (Sigma-Aldrich, St. Louis) and 4 ng/ml human basic fibroblast growth factor (bFGF) (R&D). Undifferentiated iPSCs were characterized by positive staining of Oct3/4, Nanog, SSEA-3 and TRA1-60.

To derive NCSCs, iPSCs were grown as embryo body (EB)-like floating cell aggregates in ESC maintenance medium without bFGF for 5 days. The cell aggregates were cultured in a serum-free neural induction medium (SFM) consisting of Knockout DMEM/F12, StemPro neural supplement (Invitrogen), 1% GlutaMAX™-I (Invitrogen), 20 ng/ml bFGF and 20 ng/ml EGF for 10 days. At day 15, cells migrating from rosettes differentiated into NCSCs. Alternatively, cell clusters were mechanically harvested and cultured in SFM suspension for 7 days to form a spherical structure. The cells migrating

out of the colonies were re-plated (NCSC passage 1; P1) and maintained in the SFM. NCSCs characterization was examined by immunofluorescent staining of NCSCs markers (HNK1, P75, Vimentin and Nestin). Assays for NCSCs differentiation to neural and mesenchymal lineages demonstrated cell multipotency as described previously [16,18].

4.2.2. Bi-layer Nanofibrous Vascular Scaffold Fabrication

Nonwoven aligned nanofibrous vascular scaffolds composed of Poly-(L-lactide) PLLA (1.09 dl/g inherent viscosity) (Lactel Absorbable Polymers Inc, Pelham, AL) were fabricated using a customized electrospinning process. The aligned nanofibrous vascular scaffold was comprised of a luminal region of longitudinally aligned nanofibers and an outer region of circumferentially oriented nanofibers. PLLA was dissolved in a volatile organic solvent, hexafluoroisopropanol (HFIP) (Matrix Scientific, Columbia, SC). The electrospinning apparatus consisted of a syringe pump capable of delivering the polymer solution to the tip of a needle secured onto a mechanized platform suspended over a 1mm outer diameter rotating mandrel collector assembly. The needle platform was charged by a positive-polarity power supply and the mandrel assembly was charged by a negative-polarity power supply. To make the inner layer with aligned nanofibers, the jet stream of PLLA (19% weight/volume) solution from the spinneret whipped between the two conductive ends of a plastic mandrel, resulting in aligned nanofibers on the non-conductive portion in the middle of a slowly rotating mandrel. The outer layer with random nanofibers was generated by increasing the rotating speed of the mandrel to 800 rpm.

Upon completion of electrospinning, the nanofibrous vascular scaffolds were air dried on the mandrel collector for two nights to remove residual HFIP. The vascular scaffolds were then rinsed in deionized water and cut to appropriate length. All vascular

scaffolds were sterilized with ethylene oxide gas before characterization and *in vivo* implantation studies. The alignment of nanofibers and the structure of the nanofibrous scaffolds were examined by a Hitachi TM-1000 scanning electron microscope (SEM) (Hitachi U.S.A., Schaumburg, IL). The diameter of nanofibers ranged from 500-800 nm.

4.2.3. Matrigel-Cellular Scaffold Fabrication

Tubular conduits of inner diameter 2.5cm with random fibers were fabricated by the electrospinning method. NCSCs were detached by TrypLE and re-suspended in the SFM (2×10^4 cells/μl). The cell suspension was mixed with cold matrigel solution at 2:1 ratio (volume to volume), and injected into the longitudinally opened conduit (e.g., 100 ml for one 2.5 cm conduit). The constructs were kept in the incubator for more than an hour, and NCSC maintenance medium was added to cover the constructs. The culture was maintained in the incubator overnight before surgery. The matrigel was removed from the conduit and wrapped around the vascular scaffold during the surgery.

4.2.4. Collagen-Cellular Scaffold Fabrication

The collagen gel constructs were made with a final composition of 1milligram per milliliter of collagen and a cell density of 4 million cells per milliliter (Table 4.1.). Appropriate amounts of 0.1 N NaOH and StemPro NSC-SFM medium with TGF-β (5ug/ml) were added to neutralize the final solution, and all solutions were kept on ice.

To construct the collagen-cellular vascular scaffold, 2% agarose gel, a 15 mL tube and a 1 mL syringe with a needle were required. 6 milliliters of 2% agarose gel were added to the 15 mL tube, which was allowed to partially polymerize on ice. The 1 mL

syringe with a needle was placed into the polymerized agarose gel on ice. 500 microliters of 2% agarose gel were then added into the 1 mL syringe and allowed to polymerize on ice. The sterilized scaffolds placed on a mandrel were inserted into the 1 mL syringe with the edge of the scaffold resting on the top of the agarose gel (Figure 4.7.). The collagen gel with NCSCs was added into the 1 mL syringe until the solution (125ul, 1 million cells) fully covered the vascular scaffold. After incubation and polymerization in a 37°C, 5% CO_2 incubator for 1 hour, medium with TFG-β was added

Solution	Volume (µL)
KO DMEM / F-12 w/ TGF-β and NCSCs	340
0.1 N NaOH	27.5
Collagen I (3.68 mg/mL)	137.7
Total	500

Table 4.1. Appropriate amount of solution in collagen gel fabrication.

and the gel was allowed to contract for 24 hours. Following the 24 hour incubation, the vascular scaffolds were implanted into adult athymic rats.

Live/Dead assay (Molecular Probes, Eugene, Oregon) was used to assess the viability of the NCSCs after the surgery for vascular scaffold implantation. Briefly, the samples were harvested and then incubated in the culture medium containing 4mM ethidium bromide (stains dead cells) and 2mM calcein (stains live cells) for 1.5 hours at 37°C. The samples were then fixed in 4% paraformaldehyde and immediately visualized using a Nikon TE300 fluorescence microscope.

4.2.5. *In vivo* Implantation

All animal study procedures were approved by the Institutional Review Board Service and Institutional Animal Care and Use Committee at the University of California, Berkeley. Adult athymic rats (200 ± 20 g) were anesthetized with 1.5% isoflurane in 70% N_2O/30% O_2. Body temperature was maintained at 37.0±0.5°C during surgery.
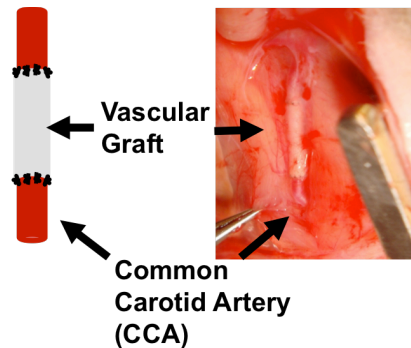

Figure 4.1. Nanofibrous vascular graft with NCSCs after three months of implantation.

Briefly, the rat was set in a supine position, and a midline incision was made on the ventral side of the neck to expose the left common carotid artery (CCA). Under a surgical microscope, the carotid artery was isolated and the segment of the artery was clamped temporarily. A nanofibrous vascular scaffold was placed end-to-end to the CCA and sutured with 10-0 interrupted stitches. Retrieval of the scaffold involved the same initial steps for implantation. The vascular scaffold was removed by ligation of native CCA directly adjacent to the suture locations. The incised muscle layers were approximated with interrupted 4-0 nylon sutures and stainless steel wound clips were used to close the skin wound.

The animals were divided into experimental groups according to the composition of the implanted vascular scaffold as follows: nanofibrous vascular scaffold only (n=15), Matrigel-cellular vascular scaffold (n=15) and Collagen-cellular vascular scaffold (n=15). The animals were sacrificed at 2 weeks, 1month and 3 months post-surgery.

4.2.6. Mechanical Testing

Nanofibrous vascular scaffolds were subjected to load-to-failure testing to determine their Young's modulus mechanical strength. The animals were sacrificed and scaffold samples were explanted. Briefly, the scaffold was cut into 1.5-2 mm long segments, mounted on the Instron mechanical test system and subjected to uniaxial loading (Figure 4.2.) to failure at a strain rate of

Figure 4.2. Mechanical testing of the segment excised from a vascular scaffold.

0.0025/s. Young's modulus was obtained from the slope of the linear part of the stress-strain curve. At least 3 samples for each group were tested to calculate the mean and SD.
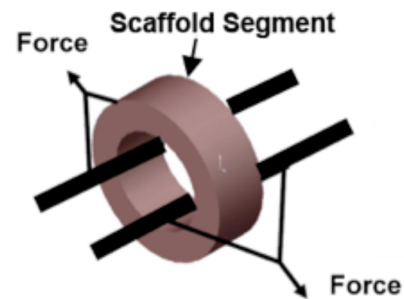
4.2.7. Histological Evaluation

For histological analysis, the sample was placed into OCT and cryopreserved at -20°C. The frozen cross-sections (10 μm in thickness) were fan-dried for 1 hour at room temperature. Then the slides were fixed in 4% paraformaldehyde solution for 15 minutes at room temperature. Samples were incubated in 5% normal goat serum for 30 minutes to block the non-specific binding, and then incubated overnight at 4°C with primary antibody diluted in 5% normal goat serum. Primary antibodies include anti-CD31 (1:100 dilution, BD Pharmigen) for endothelial cells (ECs), anti-neurofilament (1:200 dilution, Sigma) for axons, anti-glial fibrillary acidic protein (GFAP) (1:2000 dilution, Sigma) for astrocytes, anti-myosin heavy chain (MHC) (1:50 dilution, Santa Cruz) and α-actin (1:100, Sigma) for smooth muscle cells, anti-NG2 (1:100 dilution, Sigma) for pericyte, anti-Tuj1 (1:100 dilution, Millipore, Billerica, MA) for neural stem cells. Negative

controls were conducted by omitting the primary antibody. The sections were incubated for one hour with either horseradish peroxidase-conjugated anti-mouse or rabbit IgG (1:1000, Alexa 594 for red and Alexa 488 for green, Invitrogen, Carlsbad, CA). Finally, slides were mounted and examined by using a fluorescence microscope (Zeiss Axioskop 2 MOT).

Collagen and elastin were stained with Verhoeff's Elastic Stain Kit (American Master*Tech Scientific, Inc.). The sections were stained following a standard H&E staining protocol.

4.2.8. Statistical Analysis

The data are presented as mean ± standard deviation (SD). For data of mechanical test requiring comparisons between more than two groups, analysis of variance (Statview 5.0) was first used to compare differences among all groups. Post-hoc testing was performed to analyze the data by using Fisher's protected least significant difference (PLSD). A P-value less than 0.05 was considered statistically significant.

4.3. RESULTS

4.3.1. Characterization of iPSC-derived NCSCs

Four human iPSC lines (BJ1-iPS1 derived from skin fibroblasts, ADAfE4-iPS38-2 derived from skin fibroblasts, MSC-iPS1 derived from bone marrow mesenchymal stem cells) were applied in this study. NCSCs were induced from undifferentiated iPSC-derived neural rosette structures. After cell maintenance and expansion for 7-8 days, the expression of NCSC markers p75, HNK1, nestin and vimentin were shown

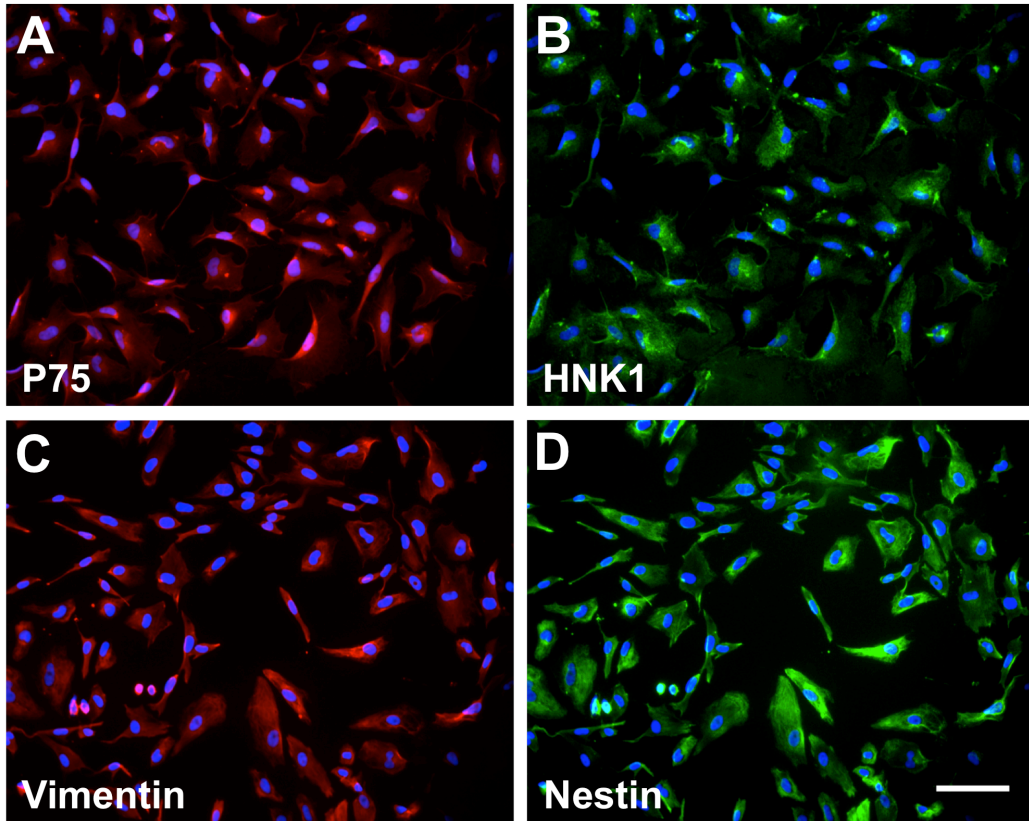homogeneously in those three NCSC lines. (Figure 4.3.)

Figure 4.3. NCSCs stained for NCSC markers Nestin, Vimentin, P75 and HNK1, indicating their NCSC identity. Nuclei were stained with DAPI (in blue). Scale bar = 100 μm.

4.3.2. Characterization of Nanofiber Organization in Vascular Scaffolds

Electrospun nanofibrous vascular scaffold with an inner diameter of 1mm were produced (Figure 4.3.A.). SEM images of the luminal surfaces showed longitudinally aligned nanofibers. Layers of circumferentially aligned nanofibers were generated outside of the longitudinally aligned nanofibers. (Figure 4.3.C-D). The purpose of longitudinally aligned fibers in the inner layer (~30 μm in thickness) was to provide guidance for the growth and migration of endothelial cells and facilitate cell infiltration into the three-dimensional (3D) scaffold. The outer layer (~70 μm in thickness) with

circumferentially aligned nanofibers enhanced the extracellular matrix remodeling and mechanical properties of the scaffolds.
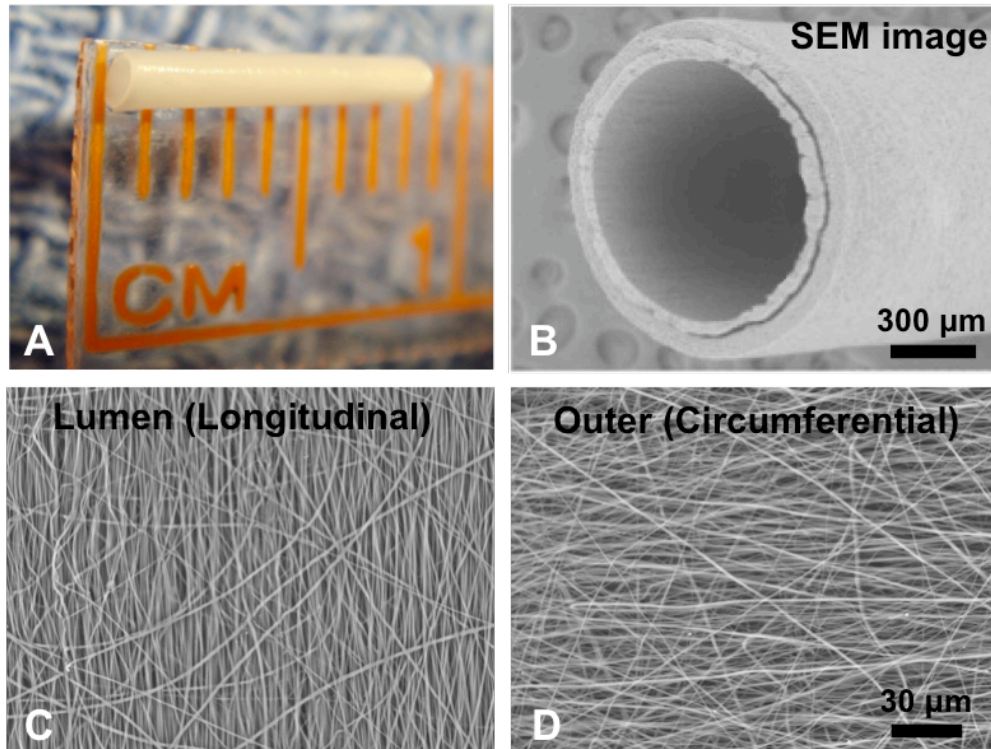

Figure 4.4. Nanofibrous Vascular Scaffold Fabrication and Characterization (A) A nanofibrous vascular scaffold (8mm length, 1mm ID). (B-D) SEM image of a vascular scaffold showing longitudinally aligned fibers in luminal layer and circumferencially aligned fibers in outer layer.

4.3.3. Multipotent Differentiation of iPSC-derived NCSCs

The differentiation of iPSC-derived NCSCs into peripheral neural cells and mesenchymal cells was assessed as previously described ([12-13]. NCSCs differentiated into Tuj+/Peripherin+ peripheral neurons in neural differentiation medium with a combination of BDNF, GDNF, NGF and dibutyryl cyclic AMP (dbcAMP) for 4 weeks. GFAP+/S100β+ Schwann cells were induced by CNTF, neuregulin 1β and dbcAMP. Besides the peripheral nerve system lineages, NCSCs were differentiated into

various mesenchymal lineages. Under specific conditions [16,18], iPSC-NCSCs differentiated into chondrocytes, osteoblasts, adipocytes and smooth muscle cells (data not shown). These results demonstrated the multipotency of derived NCSCs.

4.3.4. Mesenchymal Lineage Differentiation in NCSC Vascular Scaffolds

To assess the mesenchymal differentiation of NCSCs after vascular scaffold replacement *in vivo*, immunofluorescent staining of α-actin, MHC and NG2 was performed in NCSCs vascular scaffold samples at 2 weeks, 1 months and 3 months (Figure 4.5.). We found that many NuMA+/α-actin+ and NuMA+/MHC+ cells attached to
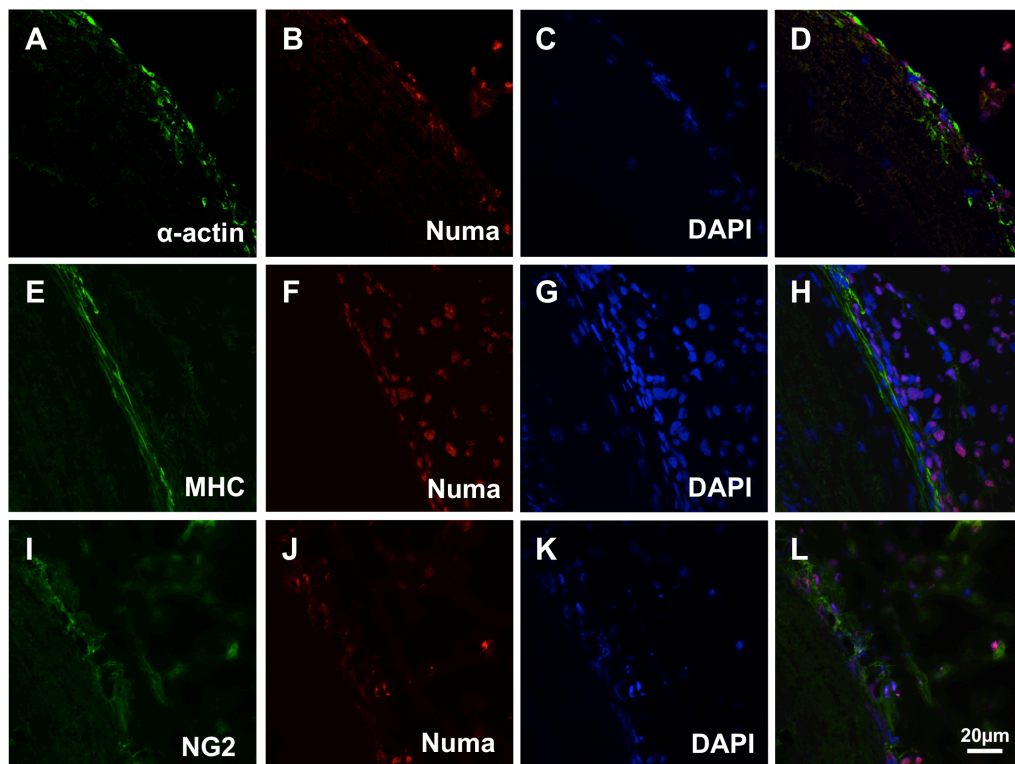

Figure 4.5. Immunofluorescent staining of mesenchymal lineage markers α-actin (A), MHC (E), and NG2 (I) (green) and human nuclei antigen NuMA (B, F, J) (red) in the cellular vascular graft transplantation group at 3 months. Cell nuclei were labeled with DAPI staining (C,G, K). The combined fluorescent staining is shown in D,H and L. Scale bar = 20 μm.

the outer surface of the vascular scaffold and formed smooth muscle cell layers with host cells. No α-actin and MHC positive staining were found to colocalize with NuMA positive cells distributed in the surrounding tissue of vascular scaffold. Interestingly, there is no positive staining of α-actin and MHC in the implanted NCSCs at 2-week and 1-month time points. In those samples only host cells were involved in the smooth muscle cell layer remodeling. In addition, NuMA+/NG2+ cells were found in both the outer surface and surrounding tissue of the vascular scaffold at 3-month time point.

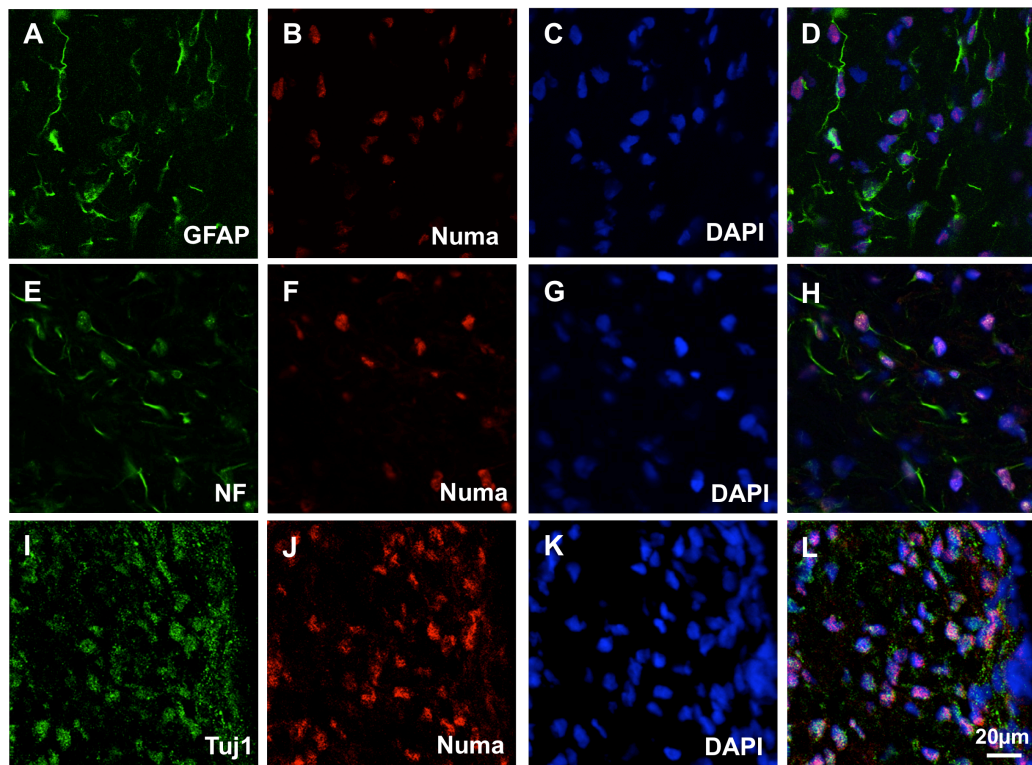**Figure 4.6. Immunofluorescent staining of peripheral neural lineage markers** GFAP (A), NF (E), and Tuj1 (I) (green) and human nuclei antigen NuMA (B, F, J) (red) in the cellular vascular graft transplantation group at 3 months. Cell nuclear was labeled with DAPI staining (C, G, K). The combined fluorescent staining was shown in D,H and L. Scale bar = 20 μm.

4.3.5. Peripheral Neural Lineage Differentiation in NCSCs Vascular

Scaffolds

To assess the peripheral neural differentiation of iPSC-derived NCSCs *in vivo*, immunofluorescent staining of GFAP, NF and Tuj1 was performed in NCSC vascular scaffold samples at 2 weeks, 1 months and 3 months (Figure 4.6.). In the surrounding area of the vascular scaffold, NuMA positive cells showed different expression of neural lineage markers including GFAP, NF and Tuj1 at the 3-month time point. No neural lineage markers were found in 2-week and 1-month samples. Moreover, no GFAP, NF and Tuj1 positive cells attached to the surface of the scaffold.

4.3.6. Cellular Graft Fabrication and Characterization

To improve the outer layer remodeling and mechanical strength in the vascular scaffold, we used collagen gel with NCSCs to wrap the scaffold tightly. The contraction of collagen gel with NCSCs around the nanofibrous scaffold can be seen in Figures 4.7.A-B. The inclusion of TFG-β in the media for the collagen gel led to better and more uniform contraction of collagen around the nanofibrous scaffolds. Live/dead assays were
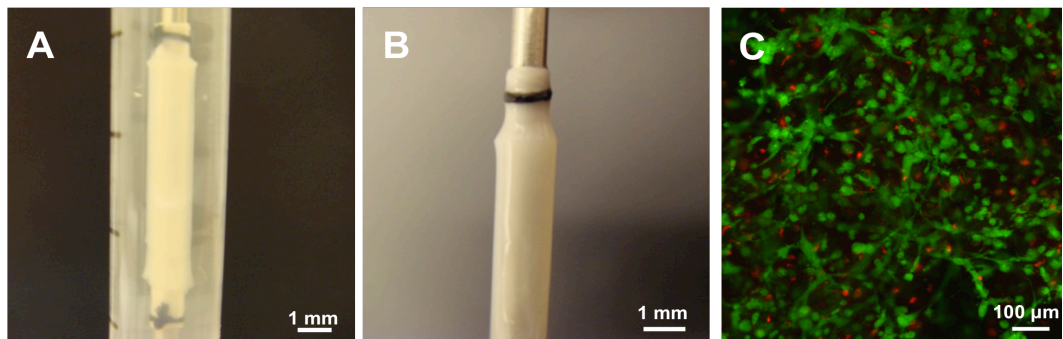

Figure 4.7. Collagen-cellular vascular scaffold fabrication. (A-B) Collagen gel layer with NCSCs wrapped around the nanofibrous vascular graft. Scale bar = 1 mm. (C) Live/dead assay after cellular vascular graft fabrication. Green = calcein-positive (live) cells. Red = ethidium bromide-positive (dead) cells. Scale bar = 100 μm.

performed to determine whether cells survived after the fabrication process and surgical procedures. After a one-day incubation period post collagen gel formation, almost all the cells were calcein positive (live) and ethidium bromide negative (dead) (data not shown). This finding suggested that the cells were not detrimentally affected by the collagen gel formation and were viable at the pre-implantation period. Another live/dead assay was performed on the NCSC vascular scaffold after *in vivo* implantation to determine the viability of the cells after the suturing procedure. Almost all the cells were calcein positive and ethidium bromide negative post surgery, indicating that they were viable in all stages during implantation (Figure 4.7.C).

4.3.7. Structure of Cellular Vascular Grafts

To evaluate the structure and cell infiltration of the vascular scaffold and surrounding tissue, hematoxylin and eosin staining was performed in acellular and cellular samples at 2 weeks, 1 month, and 3 months. Some cells infiltrated into both the acellular and cellular vascular scaffold. Most cells grew in the lumen and outer surface area, and few cells survived in the middle part of the scaffold. The loose tissue structure covered the acelluar scaffold and only a few cells penetrated into that area at the 2-week time point (Figure 4.8.A). Compared to the acelluar scaffold group, a tight tissue layer with dense cell infiltration was found in the cellular collagen group (Figure 4.8.B). After two more weeks, H&E staining showed no significant difference in the structural organization of the surrounding tissue. A thin tissue capsule enfolded the whole scaffold in the acellular scaffold group after 3 months of implantation (Figure 4.8.C). However, the cellular collagen scaffold group showed a thicker and denser tissue capsule than that of the acellular scaffold group (Figure 4.8.D). In addition, slight intimal hyperplasia was found in both the acellular and cellular collagen groups at the 3 month-time point, but not at the 2-week and 1-month time points.
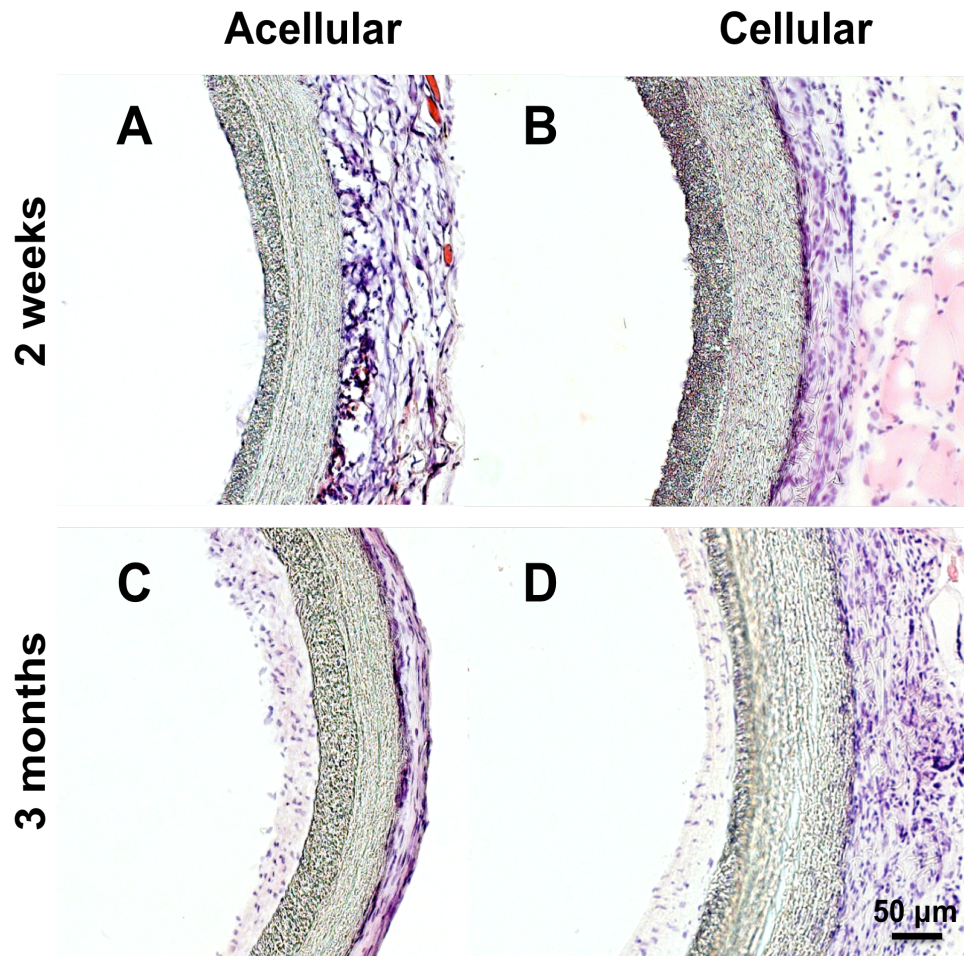
Figure 4.8. Hematoxylin and eosin staining of acellular and collagen-cellular vascular scaffold groups at 2 weeks and 3 months. A capsule layer covered the outer surface of scaffold. Scale bar = 50 µm.

4.3.8. Cellular Vascular Graft Improved Matrix Remodeling

To evaluate the structural remodeling of the cellular vascular scaffold, CD31 and MHC staining were performed to assess the smooth muscle cell layer and vascular network in acellular and cellular samples at 2 weeks, 1 month, and 3 months. After 1 month of vascular scaffold implantation, only a few CD31 and MHC positive cells were found in both acellular and cellular collagen vascular scaffold groups (Figure 4.9.A, C).

Many CD31 positive cells shown around the capsule layer represented new microvessel formation in the cellular collagen scaffold group (Figure 4.9.B). Moreover, another thicker smooth muscle cell layer covered the capsule layer in the cellular collagen group as opposed to acellular groups (Figure 4.9.D).
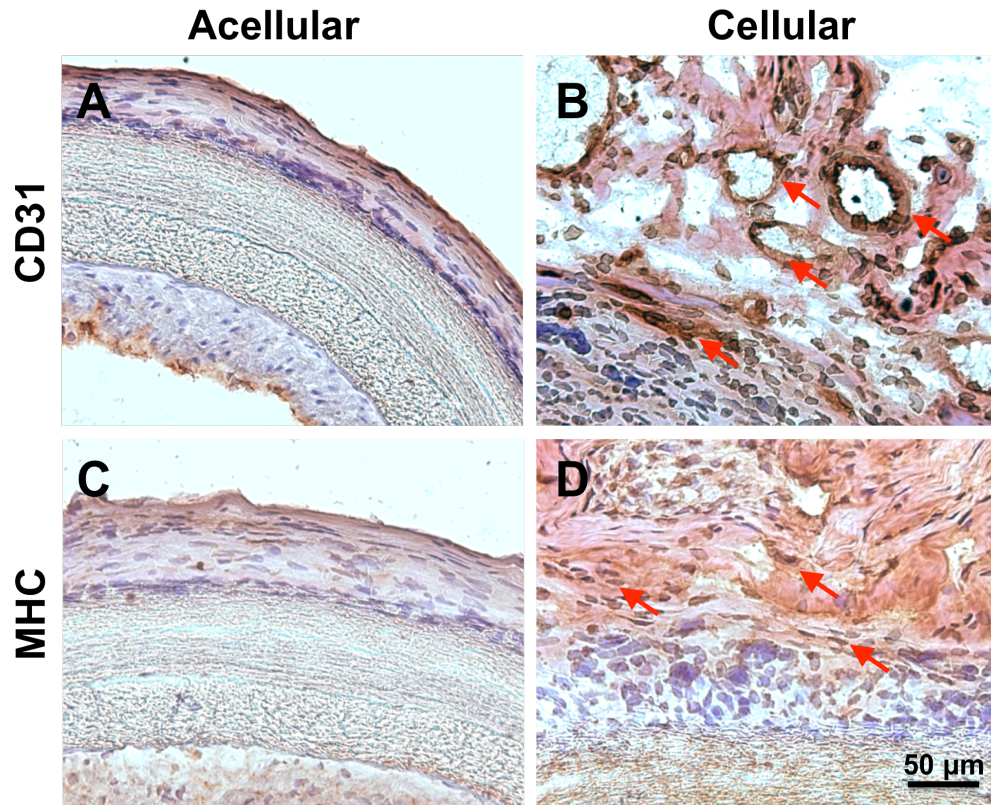
Figure 4.9. CD31 and MHC staining for acellular and collagen-cellular vascular scaffold samples at 3 months. Arrows show positive staining of CD31 and MHC. Scale bar = 50 μm.

4.3.9. Mechanical Testing of Vascular Scaffolds

The ultimate Young's modulus of the collagen-cellular vascular scaffold was 34.3±11.1N and 49.8±8.1N 1 month and 3 months after implantation, respectively. Comparatively, the average ultimate modulus of the acellular vascular scaffold was

18.7±4.4N and 31.7±3.7N 1 month or 3 months after implantation, respectively (Figure 4.10.). There was no significant difference between the acellular and collagen-cellular vascular scaffold groups at 2 weeks (data not shown). At both 1-month and 3-month time points, the collagen-cellular vascular scaffolds showed better modulus results than accelular ones ($P<0.05$). The collage-cellular vascular scaffold group of 3 months had significantly higher ultimate modulus than that of other groups ($P<0.05$).
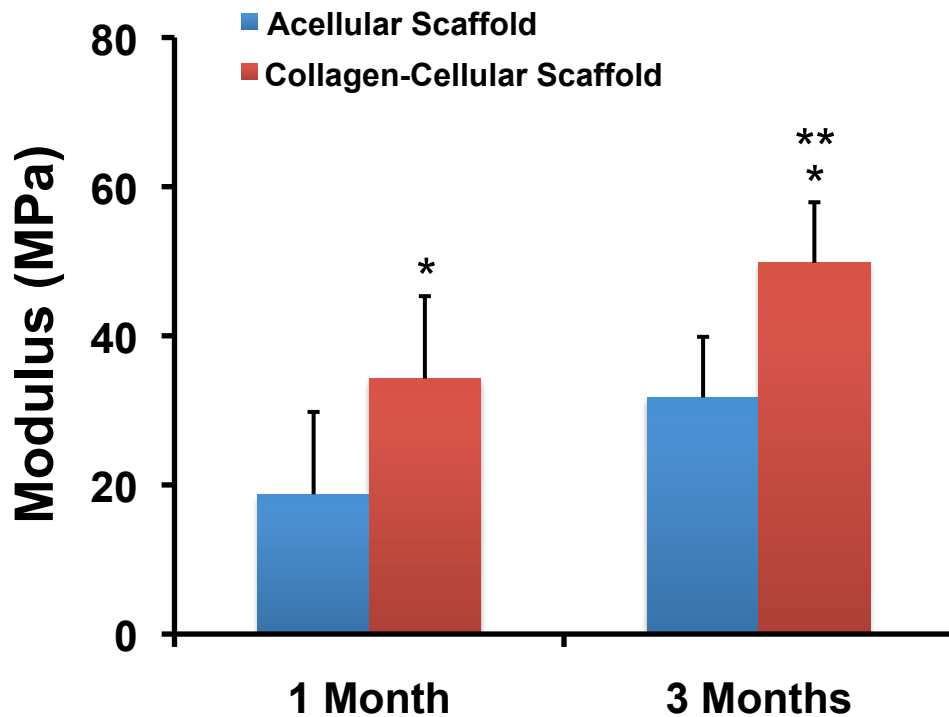

Figure 4.10. Young's Modulus of acellular and collagen-cellular scaffold samples at 1 and 3 months. * indicates significant difference ($P<0.05$) compared to acellular scaffold groups at 1-month and 3-month time point. ** indicates significant difference ($P<0.05$) compared to collagen-cellular scaffold at the 1-month time point. The data are presented as mean ± SD.

4.4. DISCUSSION

The difficulty in vascular replacement can be attributed to multiple factors, including the limited availability of venous and arterial grafts and the lack of appropriate mechanical properties and cell recruitment in synthetic vascular grafts. Most efforts to improve the strength and remodeling of synthetic vascular scaffolds have been directed toward fabricating the ideal biocompatible and biodegradable material, providing appropriate cell sources and enhancing cellular organization. Here we developed a biodegradable nanofibrous scaffold with iPSC-derived NCSCs to fabricate a novel cellular vascular graft.

To electrospin the conduits composed of aligned nanofibers, researchers in previous studies [9,19-20] either rolled a sheet with aligned nanofibers to form a vascular graft or filled a silicone tube with aligned nanofiber films. Here we developed a one-step electrospinning process to fabricate a novel, seamless, tubular nanofibrous vascular scaffold composed of two fully-integrated layers: a luminal layer with longitudinally aligned nanofibers and an outer layer with circumferentially organized nanofibers. Longitudinally aligned fibers in the lumen mimic the structure of native artery and promote endothelial cell attachment and migration. The circumferential nanofibrous layer facilitates the organization of SMCs and extracellular matrix (ECM) remodeling, to improve the mechanical properties. Natural polymers such as collagen and elastin could create a vascular graft with favorable mechanical properties and cellular integration [21-22]. The combination of synthetic polymer PLLA and collagen gel with stem cells could provide a synergistic effect on biomechanical strength and structural remodeling.

The key discovery of iPSCs reprogrammed from adult cells could create many embryonic stem (ES) like cell lines and further differentiate them into cells of interest in cellular therapies. In previous studies, we successfully differentiated different iPS cell lines to NCSCs, and four surface markers (P75, HNK1, Vimentin and Nestin) were

90

examined to demonstrate the NCSCs' identity and homogeneity. In addition, in vitro studies showed that iPSC-derived NCSCs differentiated into mesenchymal lineages (smooth muscle, chondrogenic, adipogenic and osteogenic cells) and neural lineages (Schwann cells and peripheral neurons) under different differentiation conditions.

To investigate the NCSCs' differentiation *in vivo*, the engraftment of the NCSCs with matrigel and collagen gel was implanted in a vascular healing environment for 2 weeks, 1 months and 3 months. Interestingly, the NCSCs on the surface of the scaffold expressed the positive staining of α-actin, MHC and NG2. The surrounding cellular-gel area of the scaffold showed some NG2 positive cells, but without α-actin and MHC. Moreover, we found positive GFAP, NF and Tuj positive cells only in the surrounding tissue. The positive staining of those markers is only shown at the 3-month time point, not at 2-week or 1-month. In response to various rigidity matrices, stem cells specify lineage and commit to elasticity-sensitive phenotypes [23-25]. Three months after implantation, soft matrices induced the NCSCs to differentiate to neural lineages in the vascular remodeling environment. On the contrary, rigid surfaces directed the same types of NCSCs to mesenchymal lineages, especially smooth muscle cell lines. The NCSC-derived pericytes may respond to both soft and rigid physical matrix states. In addition, no evidence of early differentiation to mesenchymal and neural lineages was *found in vivo*.

To investigate the NCSCs performance in smooth muscle cell differentiation, we used a collagen-cellular vascular scaffold model to direct NCSCs to be involved in the formation of a smooth muscle layer and facilitate cellular incorporation with the scaffold. Our results showed the cellular collagen gel wrapped around the scaffold, contracting and covering the surface of the scaffold with a dense and tight layer following TGF-β (5ng/ml) treatment (Figure 4.7.). The live/dead assay was performed after 24hrs of incubation and *in vivo* implantation to demonstrate the survival of the NCSCs and the

applicable cell seeding method. At three months post surgery, a thick tissue layer covered the scaffold, and MHC staining showed a significant smooth muscle cell layer in the collagen-cellular group. The NuMA positive NCSCs *in vivo* showed both stretched cytosol and nuclear morphology and expressed significant α-actin and MHC markers. Those implanted cells might incorporate host cells to develop the smooth muscle layer to enhance mechanical strength. Moreover, the wrapped collagen gel could be conductive to endothelial cell attachment and migration, and increased microvessel formation may encourage the local circulation to provide abundant nutrition and oxygen for cell infiltration and organization. Compared to the acellular vascular scaffold group, the results of mechanical tests showed better scaffold remodeling in collagen-cellular groups at the 3-month time point. The data of both acellular and cellular groups showed no significant difference at 2 weeks and 1 month post surgery.

Overall, this study demonstrated that nanofibrous scaffolds offer a valuable platform of cellular therapies for vascular graft replacement in addition to the guidance of SMC organization. Scaffold/gel-mediated NCSC implantation not only controlled *in vivo* differentiation to neural and mesenchymal lineages in response to various matrix stiffness conditions, but also advanced the mechanical properties. The results have imperative implications for the potential of iPSC-derived NCSCs in autologous regenerative therapies and also for understanding the physical effects of the *in vivo* vascular microenvironment.

4.5. REFERENCES

[1] Matsuda T, Miwa H. A hybrid vascular model biomimicking the hierarchic structure of arterial wall: neointimal stability and neoarterial regeneration process under arterial circulation. J Thorac Cardiovasc Surg. 1995;110:988-97.

[2] L'Heureux N, Paquet S, Labbe R, Germain L, Auger FA. A completely biological tissue-engineered human blood vessel. FASEB J. 1998;12:47-56.

[3] Seliktar D, Black RA, Vito RP, Nerem RM. Dynamic mechanical conditioning of collagen-gel blood vessel constructs induces remodeling in vitro. Ann Biomed Eng. 2000;28:351-62.

[4] Bognitzki M, Czado W, Frese T, Schaper A, Hellwig M, Steinhart M, et al. Nanostructured fibers via electrospinning. Adv Mater. 2001;13:70-+.

[5] Li D, Xia YN. Electrospinning of nanofibers: Reinventing the wheel? Adv Mater. 2004;16:1151-70.

[6] Matthews JA, Wnek GE, Simpson DG, Bowlin GL. Electrospinning of collagen nanofibers. Biomacromolecules. 2002;3:232-8.

[7] Yoshimoto H, Shin YM, Terai H, Vacanti JP. A biodegradable nanofiber scaffold by electrospinning and its potential for bone tissue engineering. Biomaterials. 2003;24:2077-82.

[8] Xu C, Inai R, Kotaki M, Ramakrishna S. Electrospun nanofiber fabrication as synthetic extracellular matrix and its potential for vascular tissue engineering. Tissue Eng. 2004;10:1160-8.

[9] Hashi CK, Zhu Y, Yang GY, Young WL, Hsiao BS, Wang K, et al. Antithrombogenic property of bone marrow mesenchymal stem cells in nanofibrous vascular grafts. Proc Natl Acad Sci U S A. 2007;104:11915-20.

[10] Park IH, Arora N, Huo H, Maherali N, Ahfeldt T, Shimamura A, et al. Disease-specific induced pluripotent stem cells. Cell. 2008;134:877-86.

[11] Ebert AD, Yu J, Rose FF, Jr., Mattis VB, Lorson CL, Thomson JA, et al. Induced pluripotent stem cells from a spinal muscular atrophy patient. Nature. 2009;457:277-80.

[12] Lian Q, Zhang Y, Zhang J, Zhang HK, Wu X, Lam FF, et al. Functional mesenchymal stem cells derived from human induced pluripotent stem cells attenuate

limb ischemia in mice. Circulation. 2010;121:1113-23.

[13] Hu BY, Weick JP, Yu J, Ma LX, Zhang XQ, Thomson JA, et al. Neural differentiation of human induced pluripotent stem cells follows developmental principles but with variable potency. Proc Natl Acad Sci U S A. 2010;107:4335-40.

[14] Grigoriadis AE, Kennedy M, Bozec A, Brunton F, Stenbeck G, Park IH, et al. Directed differentiation of hematopoietic precursors and functional osteoclasts from human ES and iPS cells. Blood. 2010;115:2769-76.

[15] Song Z, Cai J, Liu Y, Zhao D, Yong J, Duo S, et al. Efficient generation of hepatocyte-like cells from human induced pluripotent stem cells. Cell Res. 2009;19:1233-42.

[16] Lee G, Kim H, Elkabetz Y, Al Shamy G, Panagiotakos G, Barberi T, et al. Isolation and directed differentiation of neural crest stem cells derived from human embryonic stem cells. Nat Biotechnol. 2007;25:1468-75.

[17] Lam H, Patel S, Wong J, Chu J, Lau A, Li S. Localized decrease of beta-catenin contributes to the differentiation of human embryonic stem cells. Biochem Biophys Res Commun. 2008;372:601-6.

[18] Wang D, Park JS, Chu JS, Krakowski A, Luo K, Chen DJ, et al. Proteomic profiling of bone marrow mesenchymal stem cells upon transforming growth factor beta1 stimulation. J Biol Chem. 2004;279:43725-34.

[19] Kim YT, Haftel VK, Kumar S, Bellamkonda RV. The role of aligned polymer fiber-based constructs in the bridging of long peripheral nerve gaps. Biomaterials. 2008;29:3117-27.

[20] Chew SY, Mi R, Hoke A, Leong KW. Aligned Protein-Polymer Composite Fibers Enhance Nerve Regeneration: A Potential Tissue-Engineering Platform. Adv Funct Mater. 2007;17:1288-96.

[21] Caves JM, Kumar VA, Martinez AW, Kim J, Ripberger CM, Haller CA, et al. The use

of microfiber composites of elastin-like protein matrix reinforced with synthetic collagen in the design of vascular grafts. Biomaterials. 2010;31:7175-82.

[22] Buttafoco L, Kolkman NG, Engbers-Buijtenhuijs P, Poot AA, Dijkstra PJ, Vermes I, et al. Electrospinning of collagen and elastin for tissue engineering applications. Biomaterials. 2006;27:724-34.

[23] Flanagan LA, Ju YE, Marg B, Osterfield M, Janmey PA. Neurite branching on deformable substrates. Neuroreport. 2002;13:2411-5.

[24] Georges PC, Miller WJ, Meaney DF, Sawyer ES, Janmey PA. Matrices with compliance comparable to that of brain tissue select neuronal over glial growth in mixed cortical cultures. Biophys J. 2006;90:3012-8.

[25] Engler AJ, Sen S, Sweeney HL, Discher DE. Matrix elasticity directs stem cell lineage specification. Cell. 2006;126:677-89.

Chapter 5.

Conclusion and Future Directions

5.1. Conclusion

In this dissertation, nanofibrous scaffolds are applied as a model to investigate the effects of surface topography modifications, as a delivery and release platform, and with stem cells and tissue engineering by both in vitro and in vivo study.

Nanomaterials, one of the booming fields of nanotechnology, not only encourages scientists to design and construct nano-devices used in clinical diagnosis and monitoring but also promotes potential applications in regenerative medicine. The use of the electrospinning technique to generate functional nanofibrous scaffolds for replacing tissues such as nerve, spinal cord or blood vessels, is particularly exciting. Moreover, biocompatible and biodegradable polymers can be spun into nanofibers in the scaffold to provide mechanical support and guidance for cell growth. The structure and morphology of electrospun nanofibers can be manipulated to resemble that of extracellular matrix (ECM), therefore creating a more "familiar" environment for cells. In Chapters 2 through 4, we applied the electrospinning method to design three different nanofibrous scaffolds for peripheral nerve repair, spinal cord regeneration and vascular replacement, respectively.

As described in Chapter 2, a goal in neural tissue engineering is to develop synthetic nerve conduits for peripheral nerve regeneration with therapeutic efficacy comparable to that of autografts. Nanofibrous conduits with aligned nanofibers have been shown to promote nerve regeneration, but current fabrication methods rely on rolling a fibrous sheet into the shape of a conduit, which results in a graft with inconsistent size

and a discontinuous joint or seam. In addition, the long-term effects of nanofibrous nerve conduits, in comparison with autografts, are still unknown. In this study, we developed a novel one-step electrospinning process, and for the first time, fabricated a seamless bi-layer nanofibrous nerve conduit: the luminal layer having longitudinally aligned nanofibers to promote nerve regeneration, and the outer layer having randomly organized nanofibers for mechanical support. Long-term *in vivo* studies demonstrated that bi-layer aligned nanofibrous nerve conduits were superior to random nanofibrous conduits and had comparable therapeutic effects to autografts for nerve regeneration. This study may lead to the scalable fabrication of engineered nanofibrous nerve conduits for efficient nerve regeneration, and will facilitate the development of engineered tubular scaffolds for many other applications in regenerative medicine.

As pointed out in Chapter 3, the difficulty in spinal cord regeneration has been linked to inhibitory factors for axon growth and the lack of appropriate axon guidance in the lesion region. Here we developed scaffolds with aligned nanofibers for nerve guidance and drug delivery in the spinal cord. Blended polymers including Poly (l-lactic acid) (PLLA) and Poly (lactide-co-glycolide) (PLGA) were used to electrospin nanofibrous scaffolds with a two-layer structure: aligned nanofibers in the inner layer and random nanofibers in the outer layer. Rolipram, a small molecule that can enhance cAMP activity in neurons and suppress inflammatory responses, was immobilized onto the nanofibers. To test the therapeutic effects of nanofibrous scaffolds, the nanofibrous scaffolds loaded with rolipram were used to bridge a hemisection lesion in 8-week old rats. The scaffolds

with rolipram increased axon growth through the scaffolds and in the lesion, promoted angiogenesis through the scaffolds, and decreased the population of astrocytes and chondroitin sulfate proteoglycans in the lesion. Locomotor scale rating analysis showed that the scaffolds with rolipram significantly improved hindlimb function after 21 days. This investigation demonstrated that nanofibrous scaffolds offered a valuable platform for drug delivery for spinal cord regeneration.

In Chapter 4, we developed a one-step procedure to fabricate a seamless vascular scaffold with a bi-layer structure similar to native artery: the luminal surface has longitudinally aligned nanofibers for endothelial cell migration, and the outer layer has circumferentially aligned nanofibers for smooth muscle cell organization and structural support. iPSC-derived NCSCs' differentiation in various matrix stiffness conditions demonstrate the potential of combining iPSCs and nanofibrous scaffolds for vascular tissue engineering. The unique design of matrigel and collagen cellular vascular scaffolds sustains efficient cell recruitment and organization, significant synthesis and self-assembly of ECM, and excellent patency. Moreover, collagen-cellular vascular scaffolds with TGF-β show significant synthesis, self-assembly of ECM and increased mechanical strength. In this chapter, we uncovered the multi-differentiation properties of iPSC-derived NCSCs and the underlying mechanism, which may have a significant impact on the use of iPSCs for vascular tissue engineering and regenerative medicine.

In conclusion, our studies mainly focused on the new generation of prosthetic and medical implants with nanotechnology innovation, intended to benefit patient healthcare

in the long run.

5.2. Future Directions

Although significant progress has been made through this research, more detailed experiments and animal trials are necessary before the proposed designs can be used in the clinical setting.

The focus of the studies in Chapter 2 and 3 was to develop an electrospun nanofibrous scaffold with surface topographic and chemical modifications to improve its performance for peripheral nerve and spinal cord treatment. In Chapter 4, we emphasized the synergistic effects of stem cells and nanofibrous scaffolds to investigate iPSC-derived NCSC differentiation and vascular structure remodeling. Since preliminary data demonstrate the pluripotent characteristics of iPSC-derived NCSCs, future studies may apply the stem cell engineered scaffold in peripheral nerve and spinal cord regeneration. For vascular scaffold applications, we may modify the nanofibers with bioactive molecule to either attract SMC infiltration or promote EC adhesion and migration. That will aid long-term patency and structural remodeling. In addition, various homopolymers, copolymers or polymer mixtures may be tested to fabricate an ideal nanofibrous scaffold in the future.
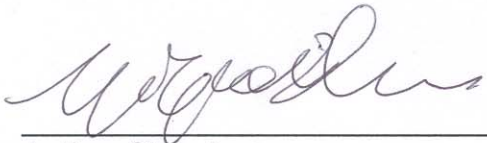
<u>UCSF Library Release</u>

Publishing Agreement
It is the policy of the University to encourage the distribution of all theses and dissertations. Copies of all UCSF theses and dissertations will be routed to the library via the Graduate Division. The library will make all theses and dissertations accessible to the public and will preserve these to the best of their abilities, in perpetuity.

Please sign the following statement:
I hereby grant permission to the Graduate Division of the University of California, San Francisco to release copies of my thesis or dissertation to the Campus Library to provide access and preservation, in whole or in part, in perpetuity.

_____   9/4/10
Author Signature   Date